Convective-Storm Environments in Subtropical South America from High-Frequency Soundings during RELAMPAGO-CACTI

RUSS S. SCHUMACHER,[a] DEANNA A. HENCE,[b] STEPHEN W. NESBITT,[b] ROBERT J. TRAPP,[b] KAREN A. KOSIBA,[c] JOSHUA WURMAN,[c] PAOLA SALIO,[d] MARTIN RUGNA,[e] ADAM C. VARBLE,[f] AND NATHAN R. KELLY[a]

[a] *Department of Atmospheric Science, Colorado State University, Fort Collins, Colorado*
[b] *Department of Atmospheric Sciences, University of Illinois at Urbana–Champaign, Urbana, Illinois*
[c] *Center for Severe Weather Research, Boulder, Colorado*
[d] *Centro de Investigaciones del Mar y la Atmósfera (CIMA/CONICET-UBA), Instituto Franco-Argentino para el Estudio del Clima y sus Impactos (UMI IFAECI/CNRS-CONICET-UBA), Departamento de Ciencias de la Atmósfera y los Océanos, FCEN, Universidad de Buenos Aires, Buenos Aires, Argentina*
[e] *Servicio Meteorológico Nacional, Argentina*
[f] *Pacific Northwest National Laboratory, Richland, Washington*

ABSTRACT: During the Remote Sensing of Electrification, Lightning, and Mesoscale/Microscale Processes with Adaptive Ground Observations-Cloud, Aerosol, and Complex Terrain Interactions (RELAMPAGO-CACTI) field experiments in 2018–19, an unprecedented number of balloon-borne soundings were collected in Argentina. Radiosondes were launched from both fixed and mobile platforms, yielding 2712 soundings during the period 15 October 2018–30 April 2019. Approximately 20% of these soundings were collected by highly mobile platforms, strategically positioned for each intensive observing period, and launching approximately once per hour. The combination of fixed and mobile soundings capture both the overall conditions characterizing the RELAMPAGO-CACTI campaign, as well as the detailed evolution of environments supporting the initiation and upscale growth of deep convective storms, including some that produced hazardous hail and heavy rainfall. Episodes of frequent convection were characterized by sufficient quantities of moisture and instability for deep convection, along with deep-layer vertical wind shear supportive of organized or rotating storms. A total of 11 soundings showed most unstable convective available potential energy (MUCAPE) exceeding 6000 J kg^{-1}, comparable to the extreme instability observed in other parts of the world with intense deep convection. Parameters used to diagnose severe-storm potential showed that conditions were often favorable for supercells and severe hail, but not for tornadoes, primarily because of insufficient low-level wind shear. High-frequency soundings also revealed the structure and evolution of the boundary layer leading up to convection initiation, convectively generated cold pools, the South American low-level jet (SALLJ), and elevated nocturnal convection. This sounding dataset will enable improved understanding and prediction of convective storms and their surroundings in subtropical South America, as well as comparisons with other heavily studied regions such as the central United States that have not previously been possible.

SIGNIFICANCE STATEMENT: Unprecedented balloon-borne measurements of the atmosphere (known as soundings) were collected in Argentina in 2018–19, during the RELAMPAGO-CACTI field projects. These measurements allowed us to characterize the conditions supporting some of the most intense thunderstorms on Earth, which are known to occur in this region. The ingredients needed for severe thunderstorms—moisture, instability, lift, and vertical wind shear—were present in several multiday episodes. The sounding data revealed that conditions were often favorable for rotating storms and large hail, but not for tornadoes. Measurements taken from mobile platforms also revealed detailed pictures of how storms influence their surroundings. This dataset will enable comparisons between storm environments in South America and other regions with intense thunderstorms that have not previously been possible.

KEYWORDS: Convective storms; Convective-scale processes; Soundings; Field experiments

1. Introduction

Subtropical South America, and in particular the La Plata basin of Argentina, has been identified as a region with some of the most intense convective storms on the planet. In particular, observations from the TRMM satellite have shown that especially deep and wide convective systems occur in this region (Zipser et al. 2006; Romatschke and Houze 2010; Liu and Zipser 2015; Houze et al. 2015), and these storms produce a very large proportion of the annual rainfall for this agriculturally productive and hydropower-dependent region (Nesbitt et al. 2006; Romatschke and Houze 2010; Rasmussen et al. 2015). Furthermore, hazardous weather, including large hail (Cecil and Blankenship 2012; Matsudo and Salio 2011; Mezher et al. 2012; Bruick et al. 2019; Kumjian et al. 2020) and heavy precipitation and flooding (Matsudo and Salio 2011; Rasmussen et al. 2015) are frequently observed.
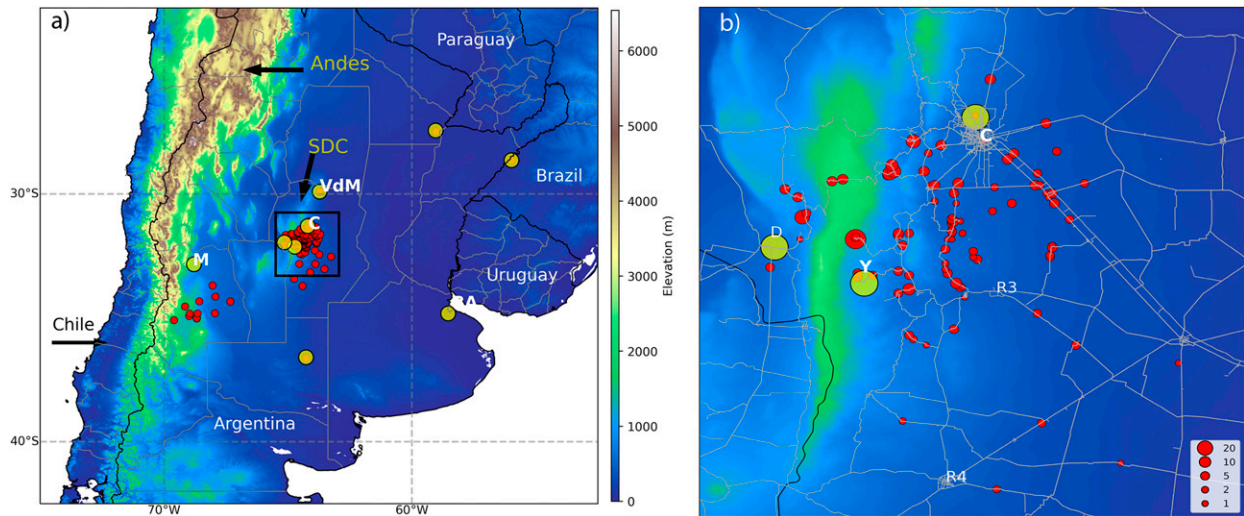
FIG. 1. (a) Elevation (m; color shading) in South America, along with the locations of RELAMPAGO-CACTI fixed sounding sites in yellow and mobile sounding locations in red. Countries are labeled, along with the Andes and Sierras de Córdoba (SDC) mountain ranges and the sounding sites of Córdoba (C), Mendoza (M), and Villa de María del Río Seco (VdM). (b) As in (a), but zoomed in on the RELAMPAGO-CACTI domain shown by the black-outlined box in (a). The sizes of symbols for mobile sounding locations are scaled according to the number of soundings collected from that location. Major roads are in gray, along with the cities of Córdoba (C), Villa Yacanto (Y), Villa Dolores (D), Río Tercero (R3), and Río Cuarto (R4).

Yet considering the importance of deep convection in this region, relatively few in situ or ground-based observations of storms and their environments are available. Operational radiosonde sites in Argentina are widely spaced, and often only take one sounding per day at 1200 UTC. Radar measurements in Argentina were driven by local efforts with very few sites available until 2015 when a new network started to slowly fill the gaps (de Elía et al. 2017). The radar data, though, have limitations for studying convective storms (e.g., Mulholland et al. 2018). These gaps in data motivated the Remote Sensing of Electrification, Lightning, and Mesoscale/Microscale Processes with Adaptive Ground Observations (RELAMPAGO; Nesbitt et al. 2021) field experiment in 2018, and its companion campaign, Cloud, Aerosol, and Complex Terrain Interactions (CACTI; Varble et al. 2021).

RELAMPAGO took place from 1 November to 18 December 2018, focused on a domain east of the Sierras de Córdoba (SDC) mountain range in Argentina (Fig. 1). CACTI had an extended observing period from 15 October 2018 to 30 April 2019, with observations primarily at an observing site in the SDC. Among the other types of in situ and remote sensing observations collected during these campaigns was a large number of balloon-borne radiosondes to observe the vertical profile of temperature, water vapor, and winds (Fig. 2). This study examines the unprecedented sounding dataset collected at fixed and mobile sites. Specifically, this is both the largest collection of soundings ever for the region, and also the first time that sounding data has been collected in a systematic manner leading up to the time when convection initiation is most frequent (1800–2100 UTC). Herein, we provide both an aggregate look at convective environments
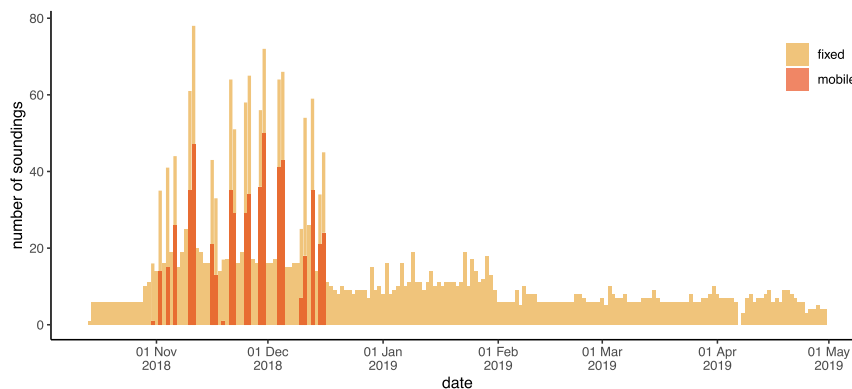

FIG. 2. Time series of the number of fixed and mobile soundings per convective day (defined from 1200 to 1159 UTC) during RELAMPAGO-CACTI.
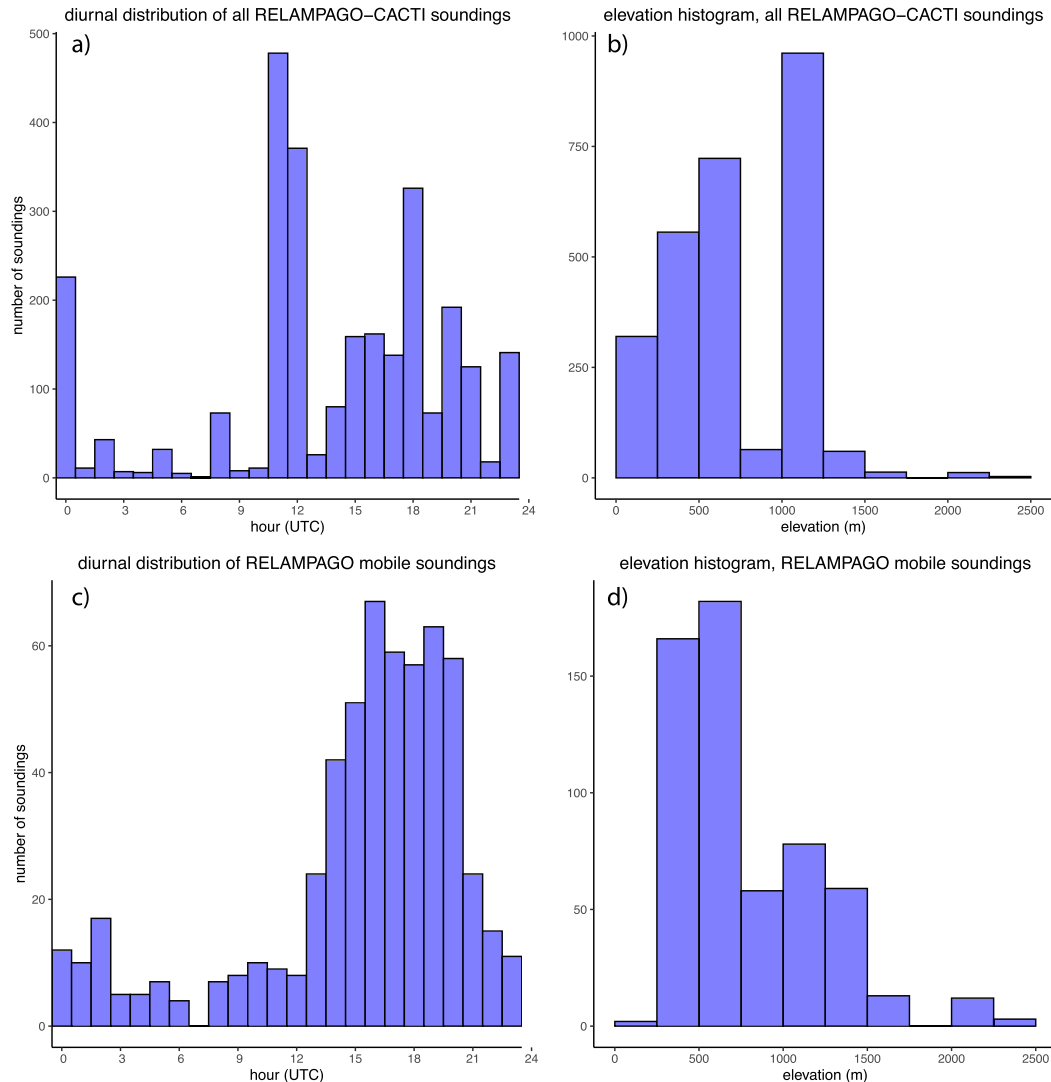
FIG. 3. The (left) diurnal and (right) elevation distributions of (a),(b) all RELAMPAGO-CACTI soundings and (c),(d) only RELAMPAGO mobile soundings (in UTC; local time = UTC − 3 h).

during RELAMPAGO-CACTI and examples of the insights that can be gained from high-frequency soundings leading up to and amid convective storms.

Section 2 will describe the observing strategies during RELAMPAGO-CACTI and the sounding dataset. Section 3 provides summary statistics of the sounding dataset, including commonly used convective and severe weather parameters. Section 4 includes brief case studies demonstrating important features observed with the soundings, including destabilization processes, the South American low-level jet (SALLJ), and convectively generated cold pools. Section 5 concludes the paper.

2. Data and methods

The RELAMPAGO-CACTI soundings are analyzed in this study using the dataset produced by NCAR's Earth Observing Laboratory (UCAR/NCAR–Earth Observing Laboratory 2020b).

This dataset was generated by processing the sounding data from different sources using a consistent processing procedure, including manual and automated quality control. This dataset includes 2714 soundings from a variety of sources, including DOE/ARM sites supporting CACTI (1255 soundings; Holdridge et al. 2018), Argentina's Servicio Meteorológico Nacional (SMN; 824 soundings; Servicio Meteorologico Nacional–Argentina 2019), a total of 577 soundings from mobile platforms from the Center for Severe Weather Research (CSWR; Center for Severe Weather Research 2019), University of Illinois (UIUC), and Colorado State University (CSU; Schumacher 2019), and Brazil's Instituto Nacional de Pesquisas Espaciais (INPE; 58 soundings; Ribeiro and Machado 2019). For analysis of the SALLJ (section 3c), a version of the dataset interpolated to a consistent vertical resolution of 5 hPa was used (UCAR/NCAR–Earth Observing Laboratory 2020a).
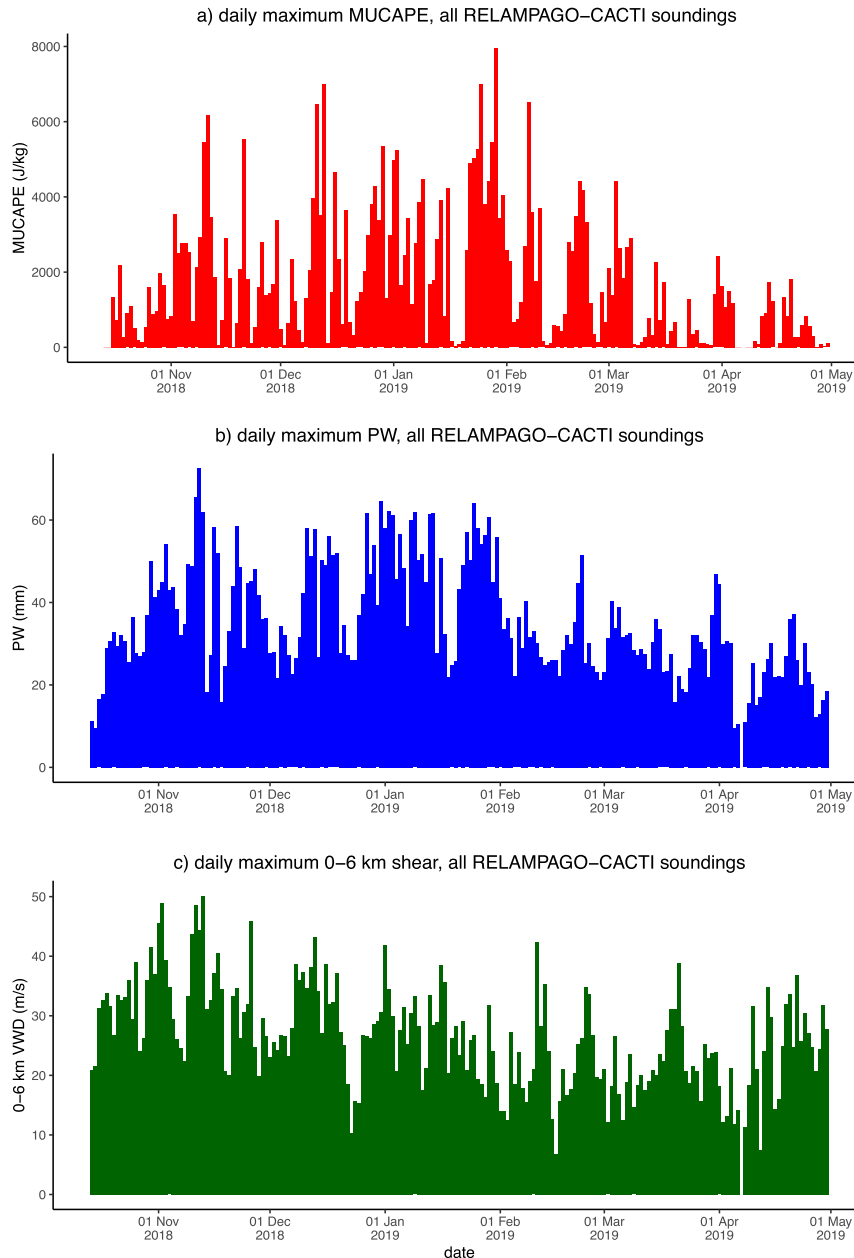
FIG. 4. Time series of the maximum observed value per convective day of (a) MUCAPE $(J\,kg^{-1})$, (b) PW (mm), and (c) 0–6-km VWD $(m\,s^{-1})$ from all RELAMPAGO-CACTI soundings. Refer to Fig. 2 for the variation in the number of samples over the campaigns. The maximum value per day does not necessarily come from the same sounding for all parameters; e.g., the maximum MUCAPE may come from one location and the maximum PW may come from another.

Fixed sounding locations included operational sites throughout Argentina (Fig. 1a), most of which launch one radiosonde per day between 1100 and 1145 UTC (nominal sounding time of 1200 UTC). However, during RELAMPAGO intensive observing periods (IOPs), the site at Córdoba launched as frequently as hourly (more commonly every 3 h) (Fig. 2). Similarly, for IOPs that occurred in Mendoza province, the operational station at Mendoza launched every 3 h.

Additionally, the site at Resistencia launched a few extra times at 0900 and 1800 UTC. Soundings from these operational sites are included in the dataset between 30 October 2018 and 31 January 2019. A special site to the north of Córdoba at Villa de María del Río Seco routinely launched a 0900 UTC sounding each day, with 3-hourly soundings during many IOPs, with a primary objective of assessing the SALLJ. DOE/ARM had two fixed sites with routine
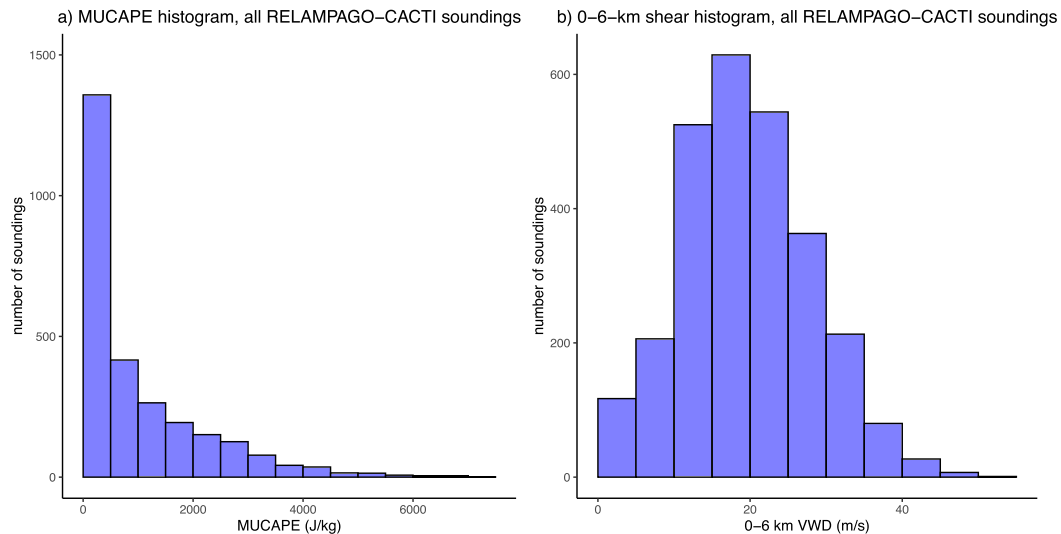
a) MUCAPE histogram, all RELAMPAGO–CACTI soundings

b) 0–6–km shear histogram, all RELAMPAGO–CACTI soundings

FIG. 5. Histograms of (a) MUCAPE (J kg^{-1}) and (b) 0–6-km VWD (m s^{-1}) for all RELAMPAGO-CACTI soundings.

radiosonde launches, one to the west of the SDC near Villa Dolores, which typically launched daily at 1200 and 1800 UTC, and one at the primary ARM observatory near Villa Yacanto, which launched daily at 0000, 1200, 1500, 1800, and 2100 UTC on days with expected deep convection and 0000, 1200, 1600, and 2000 UTC otherwise. Finally, soundings were collected by INPE at São Borja, Brazil during many IOPs when convection was expected to occur in Brazil. These fixed sounding locations all used Vaisala RS41 radiosondes. Although some of the operational sounding sites are quite distant from the RELAMPAGO domain and are thus often have differing convective environments, they are retained in the analysis here for completeness.

Radiosondes were also launched from vehicles that were positioned in advance of each RELAMPAGO IOP by the mission scientists. Detailed observing strategies were designed with the expected weather conditions and the scientific objectives of the particular mission in mind. Previous experiences in the Mesoscale Predictability Experiment (MPEX; Trapp et al. 2016) and Plains Elevated Convection At Night (PECAN; Geerts et al. 2017; Hitchcock et al. 2019) projects, along with the availability of suitable roads and launch locations guided the mobile sounding deployments. In most cases, a network of sounding vehicles was deployed across the RELAMPAGO domain, with radiosondes launched at the top of each hour for 6–8 h from the same locations. In a few cases, sounding vehicles repositioned during an IOP, either to adjust to evolving weather conditions, or to collect measurements of a specific feature such as a cold pool or a convective updraft. The large majority of IOPs took place in the primary RELAMPAGO domain in the province of Córdoba, with deployments south of the city of Córdoba both upstream and downstream of the SDC (Fig. 1b). During two IOPs the crews deployed to Mendoza province, closer to the Andes mountains (Fig. 1a). The CSWR and UIUC sounding vehicles used GRAW DFM-09 radiosondes, while the CSU system used Vaisala RS41 radiosondes.

The CSWR sounding vehicles were also equipped with vehicle-mounted surface weather observing instrumentation; the CSU vehicle had a 2-m instrumented tower that was deployed when the vehicle was stationary, and the UIUC vehicles had only handheld instruments for estimating wind speed at the surface; proximal CSWR mesonet and/or Pod observations were used for initial conditions for other variables.

To calculate various parameters pertaining to convective storms, version 1.4.0 of the Sounding and Hodograph Analysis and Research Program in Python (SHARPpy; Blumberg et al. 2017) was used. Some sounding sites reported data every 2 s, while others reported every 1 s; for consistency these were resampled to use data every 2 s. Data points within soundings that were not classified as ''good'' by the quality control system (i.e., those with a data flag greater than 1) were removed for this analysis. In two mobile soundings, the pressure measurements were flagged as in error for the entire profile. These two soundings were removed, leaving 2712 total soundings (575 mobile soundings) in the analysis.

To illustrate the sounding locations with respect to convective structures, observations from several fixed and mobile radars are also used—namely, the Doppler on Wheels (DOW) and C-Band on Wheels (COW; Center for Severe Weather Research 2019; Wurman and Kosiba 2021) radars and the Colorado State University C-Band Hydrometeorological Instrument for Volumetric Observations (CHIVO) radar (Arias and Chandrasekar 2019).

3. Summary statistics of the sounding dataset

a. Diurnal and elevation distribution

The distribution of soundings in the diurnal cycle and with respect to elevation reflect the locations and launch times of the fixed sites, with peaks in the 1100, 1200, 1800, and 0000 UTC hours (local time = UTC − 3 h) (Fig. 3a) and
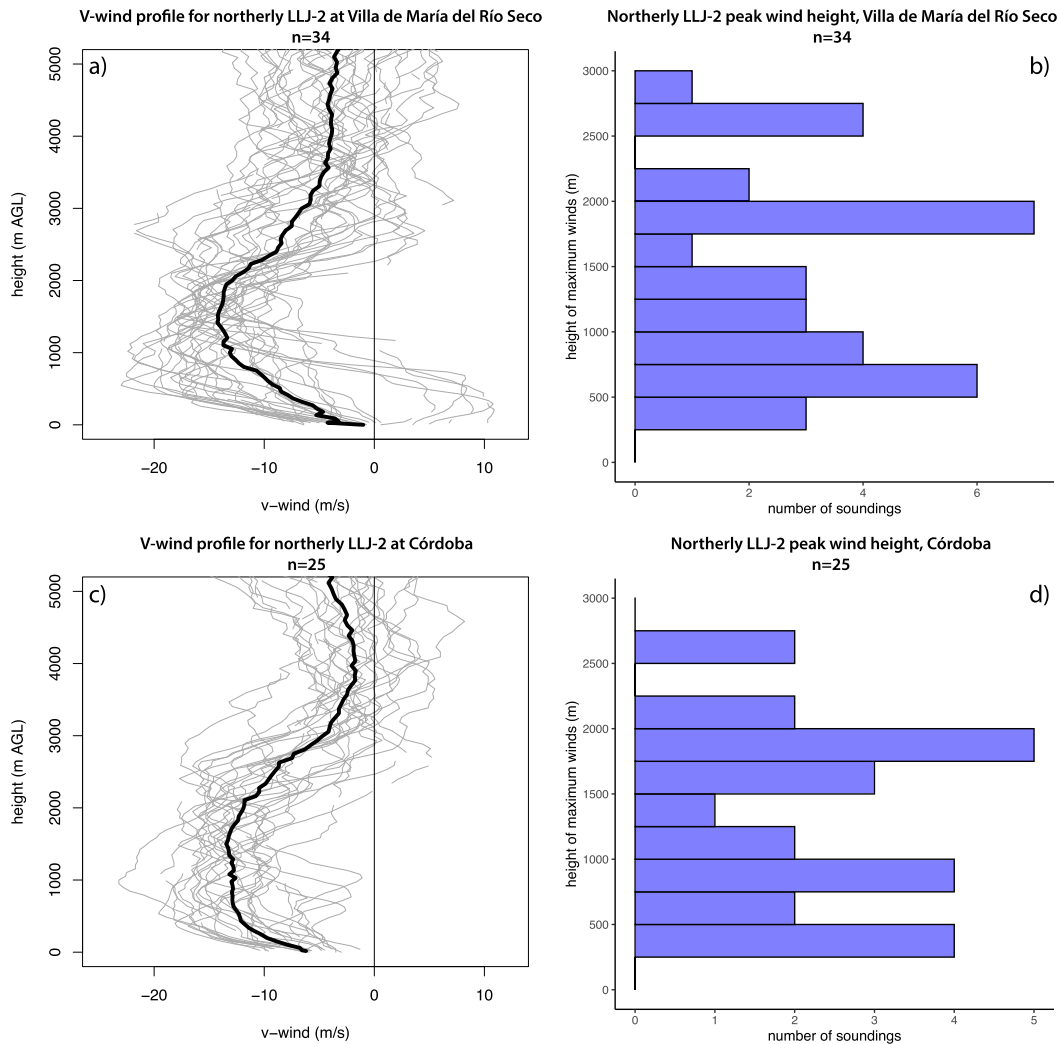
FIG. 6. Vertical profiles of the meridional wind component (m s^{-1}) for soundings meeting the northerly LLJ-2 criteria (a wind speed maximum of 16 m s^{-1} below 3 km AGL and a decrease of 8 m s^{-1} above that maximum and below 4 km AGL) at (a) Villa de María and (c) Córdoba. Individual profiles are shown in gray; the mean is shown in thick black. Also shown are histograms giving the height of the maximum wind speed for soundings meeting the northerly LLJ-2 criteria at (b) Villa de María and (d) Córdoba.

between 1000 and 1250 m (Fig. 3b), associated with the operational sounding sites and the ARM site at 1140 m MSL. Soundings at these sites took place throughout the CACTI EOP (Fig. 2). Every hour of the day had at least one sounding, though sounding times were skewed toward the daytime hours, as these were the focus of most IOPs (Fig. 3a). Aside from the ARM site, most soundings were collected at elevations below 750 m MSL, although 15 (from two different IOPs) were taken from elevations above 2000 m (Fig. 3b).

Considering only the mobile soundings, which were launched at high temporal frequency but only during RELAMPAGO IOPs in November–December 2018 (Fig. 2), the vast majority were collected between 1300 and 2100 UTC, though late-night and early morning soundings were also collected (approx. 11% of mobile soundings were taken between 0300 and 1259 UTC), with all hours except 0700–0800 UTC represented in the dataset (Fig. 3c).

Most were collected at the lower elevations east of the SDC (between 250 and 750 m MSL), though many also were taken from the foothills between 750 and 1500 m (Figs. 1b and 3d).

b. Thermodynamic parameters

With satellite observations showing that the storms in subtropical South America are among the most intense in the world, this raises the question of whether the thermodynamic environments in the region are more extreme than other parts of the world. The thermodynamic ingredients for deep moist convection—moisture and instability (e.g., Johns and Doswell 1992)—can be summarized by the convective available potential energy (CAPE). CAPE calculations are sensitive to, among other things, the level from which the parcel is assumed to be lifted. For the RELAMPAGO-CACTI soundings, we consider both the mean-layer CAPE (MLCAPE), which uses
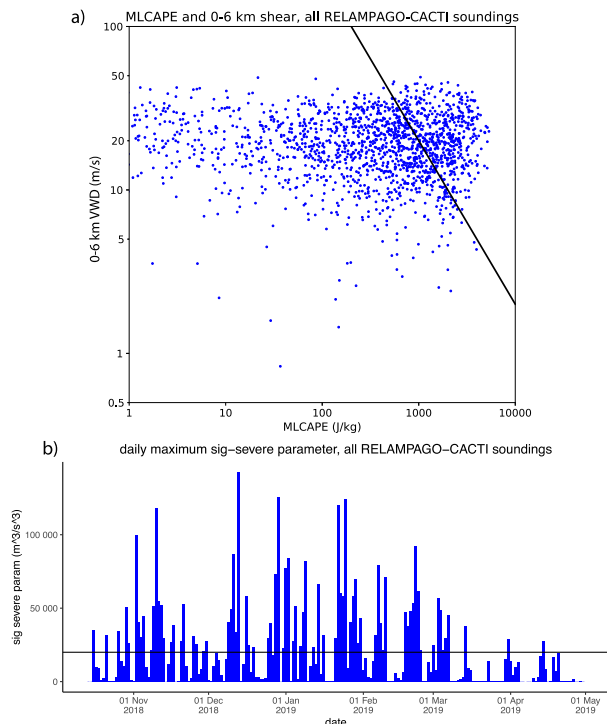
FIG. 7. (a) Scatter diagram of MLCAPE (J kg^{-1}) and 0–6-km VWD (m s^{-1}), using logarithmic axes. The black line shows the significant-severe parameter C from Craven et al. (2004), where MLCAPE × 0–6-km VWD = 20 000 m^3 s^{-3}. According to this parameter, observations to the upper right of this line are supportive of severe convective storms. (b) As in Fig. 4, but for the significant-severe parameter C.

the average properties of the lowest 100 hPa to represent the lifted parcel (e.g., Craven et al. 2002), as well as the most unstable CAPE (MUCAPE), which is the CAPE for the parcel with the greatest observed θ_e in the column, to identify the instability in cases with elevated unstable layers, though MUCAPE can also capture unrepresentative conditions (such as superadiabatic layers or very shallow moist layers) near the surface. Because some soundings, especially from the mobile platforms, were terminated prior to reaching the level of neutral buoyancy (LNB) to prepare for the launch of another radiosonde, the CAPE calculations reported here (which consider integrated buoyancy to the highest level with available data if no LNB is present) are underestimates for those soundings. For precipitable water (PW), the vertical integration is from the surface to 200 hPa or the top of the available data, whichever is lower; PW may be similarly underestimated for soundings that terminated early. Approximately 4% of all soundings in the dataset terminated below 300 hPa, and 1.5% terminated below 500 hPa.

The seasonal cycle is apparent in the time series of maximum MUCAPE from the sounding dataset, with values increasing into austral summer, peaking in late January, and declining into the autumn; within this general pattern are periods of

several consecutive days with little instability and other periods with very large MUCAPE, in excess of 6000 J kg^{-1} (Fig. 4a). The time series of MLCAPE has a very similar pattern, but with lower values as expected (not shown). The time periods with large MUCAPE generally correspond with increased PW (Fig. 4b), though the largest values of PW during the study period were observed on 12–13 November when a strong synoptic-scale trough approached the region, resulting in an active episode of convective systems (discussed further in section 4), rather than in midsummer. None of the daily maximum values of MUCAPE were from soundings that terminated below 300 hPa; four of the daily maximum values of PW were from soundings that terminated below 300 hPa. The distribution of MUCAPE has a long tail, with most soundings having CAPE < 1000 J kg^{-1}, but some extremely large values (Fig. 5a).

c. SALLJ

An important aspect of convective storm environments in subtropical South America is the South American low-level jet (e.g., Vera et al. 2006; Salio et al. 2007; Montini et al. 2019). During RELAMPAGO, a sounding site at Villa de María del Río Seco (hereinafter Villa de María), located approximately 175 km north of Córdoba (Fig. 1a), collected daily soundings at 0900 UTC, along with other times during IOPs, to monitor the SALLJ and its potential effects on convection. The objective criteria for identifying low-level jets first introduced by Bonner (1968) and modified by Whiteman et al. (1997) and Oliveira et al. (2018) were applied to the soundings taken at Villa de María, along with those from Córdoba. Namely, the vertical profile of wind speed must have a maximum exceeding 10 m s^{-1} below 3 km AGL and a decrease of at least 5 m s^{-1} above that maximum and below 4 km AGL, to reflect a "jet" profile. Of the 136 soundings collected from Villa de María during RELAMPAGO, 105 (77%) met the criteria for a low-level jet. In contrast, at nearby Córdoba, only 137 of the 270 soundings (51%) had a low-level jet. The times of day that were sampled differed considerably (a majority of Villa de María soundings were taken in the early morning when the SALLJ is near its maximum strength, whereas those from Córdoba were more evenly distributed through the day), which likely explains some of this difference; similarly the location farther north is more frequently in the core of the SALLJ (Oliveira et al. 2018).

Subsetting these soundings further to identify northerly jets meeting the Bonner/Whiteman "LLJ-2" criteria—a wind speed maximum of 16 m s^{-1} below 3 km AGL and a decrease of 8 m s^{-1} above that maximum and below 4 km AGL—reveals 34 such soundings at Villa de María and 25 at Córdoba. (There were also 9 and 17 soundings with southerly LLJs meeting these criteria, respectively. Equatorward-directed LLJs are observed in both South America and the U.S. Great Plains and typically occur after the passage of a cold front, as discussed by Bonner (1968). In the average of these wind profiles, there is a broad maximum in winds between approximately 750 m and 2 km (Figs. 6a,c). However, these mean profiles do not reflect some of the complex structures observed in individual soundings.
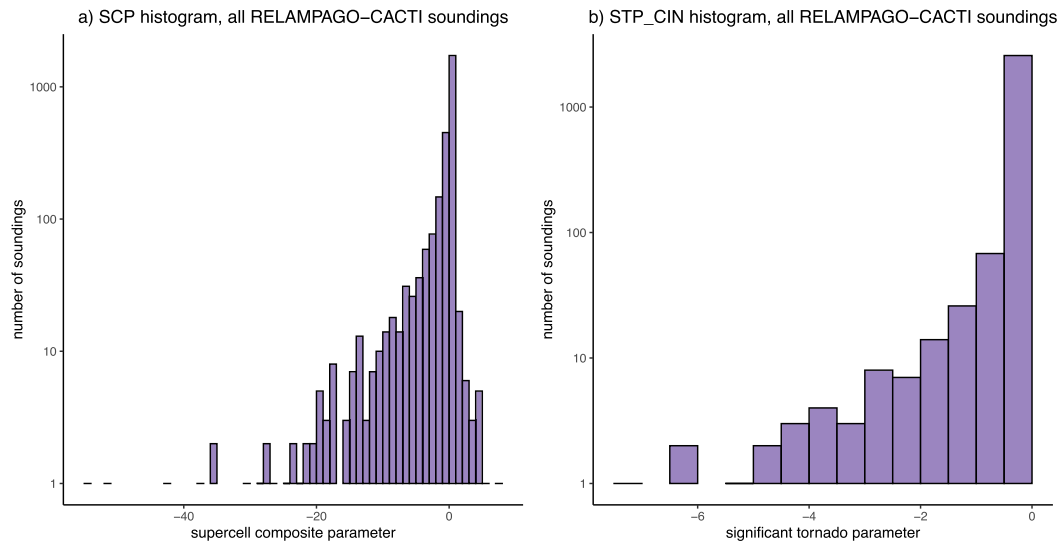
FIG. 8. As in Fig. 5, but for (a) the supercell composite parameter (SCP) and (b) the significant tornado parameter (STP). Note that the *y* axes use a logarithmic scale.

Histograms show that the height of the maximum wind speed frequently occurs below 1 km, as well as between 1.5 and 2 km, with relatively few maxima in between (Figs. 6b,d), consistent with the broad range of LLJ heights found in Argentina by Oliveira et al. (2018, their Fig. 12). Some soundings observed relatively weak winds at approximately 1 km AGL with a peak above that and others have strong near-surface southerly winds with a northerly jet above. The cases with the peak wind height below 750 m AGL are more in line with U.S. Great Plains LLJs, where the wind maximum is frequently near 500 m AGL (e.g., Whiteman et al. 1997; Song et al. 2005; Smith et al. 2019; Carroll et al. 2019). In contrast, those peaking at 1.5–2 km are located much higher than those typically observed in the United States, similar to the findings of Oliveira et al. (2018). The diurnal cycle, spatial structure, and other aspects of SALLJ observations during RELAMPAGO-CACTI are a current area of active investigation (e.g., Sasaki et al. 2021).

d. Vertical wind shear and severe-weather parameters

For organized or rotating storms to occur, vertical wind shear is necessary in addition to the basic ingredients for deep convection. One parameter that is often used to diagnose the potential for convective organization is the magnitude of the vector wind difference (VWD) between the surface and 6 km AGL (e.g., Markowski and Richardson 2010); this corresponds to vertical shear but is in units of wind speed for ease of interpretation. (Because all VWD calculations are done over a fixed depth, the term ''shear'' is used interchangeably with VWD in this manuscript.) Magnitudes of 0–6-km VWD greater than approximately $10\,\mathrm{m\,s^{-1}}$ generally support organized convective systems; values greater than $20\,\mathrm{m\,s^{-1}}$ indicate the potential for supercell storms, assuming convection initiates (e.g., Markowski and Richardson 2010).

Like the moisture and instability parameters, the daily maximum shear varied considerably over the RELAMPAGO-CACTI campaigns, with 1–5-day periods of increased wind shear interrupted by extended periods with weaker shear (Fig. 4c). The largest shear magnitudes were observed during the November–December RELAMPAGO field phase, with one sounding on 13 November exceeding $50\,\mathrm{m\,s^{-1}}$. In the dataset as a whole, the 0–6-km shear was routinely between 10 and $30\,\mathrm{m\,s^{-1}}$, with occasional values exceeding $40\,\mathrm{m\,s^{-1}}$ (Fig. 5b).

Combined with the availability of the instability required for convection, the regular presence of vertical wind shear helps to explain the frequent occurrence of organized
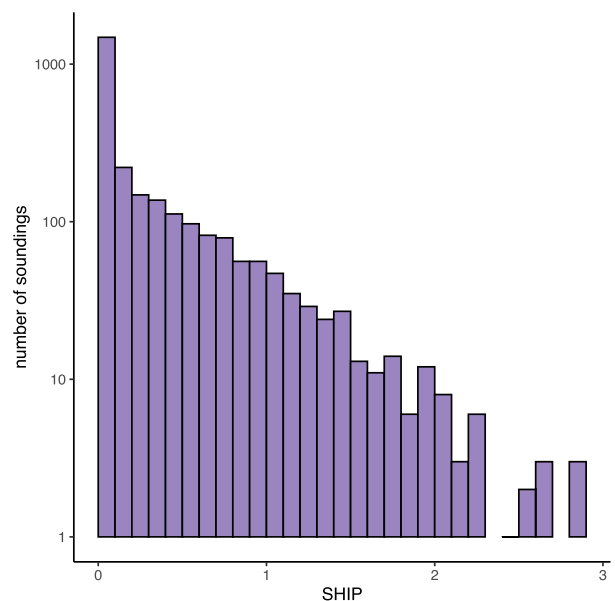

FIG. 9. As in Fig. 5, but for the significant hail parameter. Note that the *y* axis uses a logarithmic scale.
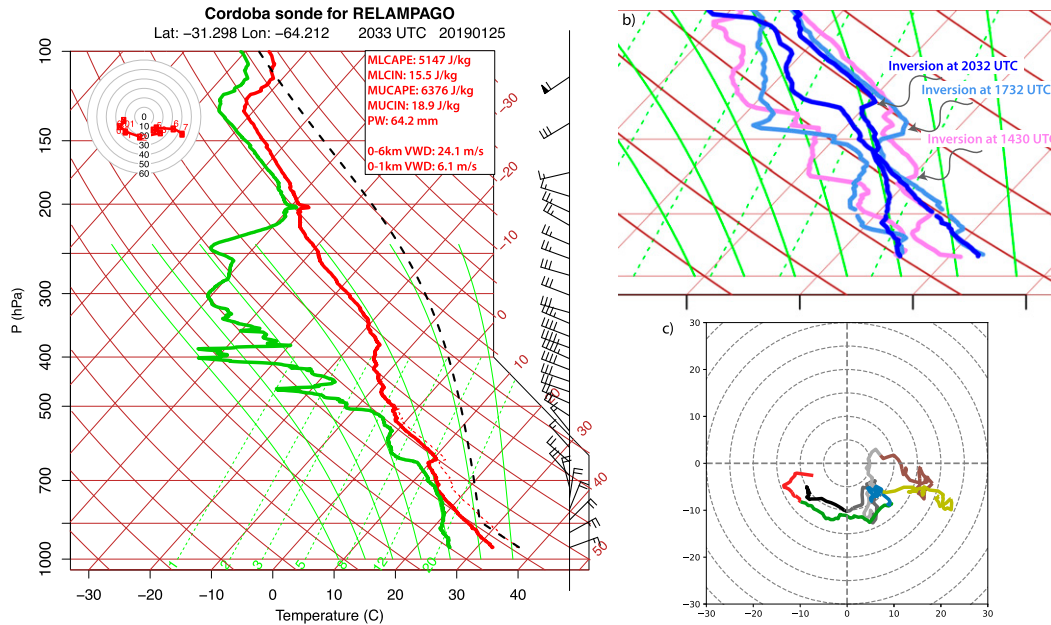
FIG. 10. (a) Skew T–log$p$ diagram of the sounding from Córdoba at 2033 UTC 25 Jan 2019. For this and all subsequent skew T–log$p$ images, the wind profiles are in knots (1 kt ≈ 0.51 m s^{-1}), with a small barb indicating 5 kt, a large barb indicating 10 kt, and pennant indicating 50 kt. The thin dashed red line shows the virtual temperature, and the thick black dashed line shows the temperature of a lifted parcel with the mean properties of the lowest 500 m AGL. (b) As in (a), but zoomed in to the layer below 500 hPa and including the Córdoba soundings for 1430 UTC (violet), 1732 UTC (light blue), and 2032 (blue). (c) Wind hodographs (m s^{-1}) for the 1732 and 2033 UTC soundings, with the 1732 UTC sounding in shades of gray/brown and 2033 UTC sounding in color. Shades change at 1, 3, and 5 km AGL.

convective storms in the region. Although the most shear did not always occur on the same days as the greatest instability (Fig. 4c), numerous soundings had sufficient instability and shear for organized and potentially severe convective storms (Fig. 7a). Indeed, using the product of the MLCAPE and 0–6-km VWD, referred to as the "significant severe" parameter C (Craven et al. 2004; Gensini and Ashley 2011), 18% of the soundings in the full RELAMPAGO-CACTI dataset were supportive of significant severe weather, with $C \geq 20\,000\,\mathrm{m}^3\,\mathrm{s}^{-3}$ (Figs. 7a,b). Furthermore, 37% of "convective days" (defined from 1200 to 1159 UTC to account for the typical diurnal cycle of convection) had at least one sounding meeting this criterion.

Considering the propensity for severe weather to occur in subtropical South America—especially large hail and, to a lesser extent, tornadoes, parameters that have been designed to diagnose a combination of severe weather ingredients may prove useful in this analysis, beyond the relatively simple significant-severe parameter. Although care must be taken in interpreting these composite parameters (Doswell and Schultz 2006), they are widely used in operational severe storms analysis forecasting in the United States and elsewhere because they synthesize

numerous individual variables in a standardized manner (Thompson et al. 2012).

One such parameter that has been shown to discriminate between environments supporting supercell and non-supercell storms is the supercell composite parameter (SCP, Thompson et al. 2004). SCP incorporates MUCAPE, and the vector wind difference and storm relative helicity over the effective inflow layer (Thompson et al. 2007; Nowotarski et al. 2020), with greater magnitudes indicating environments supportive of supercells. For this study, the SCP calculation was modified to use the negative storm-relative helicity, corresponding to a cyclonic (left-moving) supercell in the Southern Hemisphere. Although most soundings from RELAMPAGO-CACTI have near-zero values of SCP as expected, approximately 18% of all soundings have SCP < −1, and 6.7% have SCP < −5 (Fig. 8a). In total, 11 soundings had SCP < −25, which occurred on six different days. On 5 of these days, rotating storms were observed (or are presumed to have occurred based on available data); the sixth was in northern Argentina in January with limited data to confirm whether or not supercells developed.

A related parameter is the significant tornado parameter (STP; Thompson et al. 2003, 2004), defined as follows:

$$\text{effective-layer STP} = [\text{MLCAPE}/(1500\,\mathrm{J\,kg}^{-1})] \times [\text{ESRH}/(150\,\mathrm{m}^2\,\mathrm{s}^{-2})] \times [\text{EVWD}/(20\,\mathrm{m\,s}^{-1})]$$
$$\times [(2000 - \text{MLLCL})/(1000\,\mathrm{m})] \times [(200 + \text{MLCIN})/(150\,\mathrm{J\,kg}^{-1})],$$
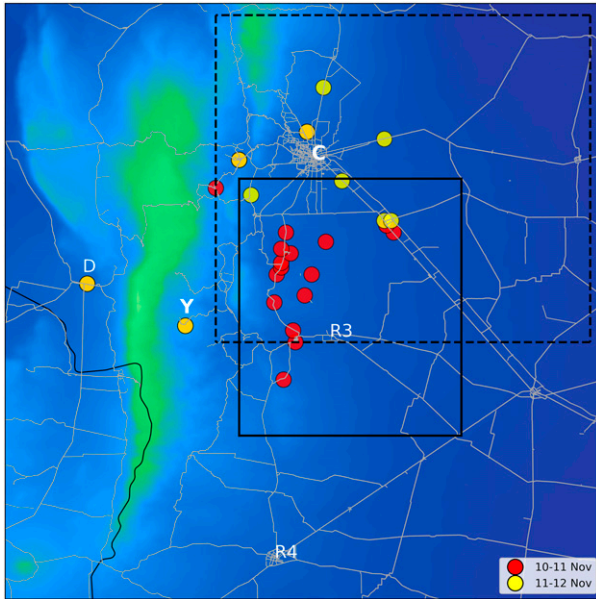
FIG. 11. As in Fig. 1b, but red circles show locations of radiosonde launches on 10–11 Nov 2018 (IOP4), yellow circles show locations of launches on 11–12 Nov 2018 (IOP5), and orange circles had launches in both IOPs. The solid-outlined rectangle indicates the area shown later in Fig. 12, and the dash-outlined rectangle indicates the area shown later in Fig. 14.

where ESRH and EVWD are the storm-relative helicity and vector wind difference over the effective inflow layer, and where the EVWD term is capped at a value of 1.5 for EVWD > 30 m s^{-1} and to 0.0 for EVWD < 12.5 m s^{-1}; the MLLCL term

is to 1.0 for MLLCL heights < 1000 m AGL and set to 0.0 for MLLCL heights > 2000 m AGL; and the MLCIN term is set to 1.0 for MLCIN > −50 J kg^{-1} and to 0.0 for MLCIN < −200 J kg^{-1}. The ESRH calculation was again modified for the Southern Hemisphere.

During the primary RELAMPAGO campaign in November–December 2018, observations of large magnitudes of STP were rare, with only four days having soundings with STP < −2 and only a single sounding with STP < −4. However, larger values of STP were more frequently observed from the fixed sounding sites in late December 2018 through February 2019 (Fig. 8b). Approximately 14% of convective days in the full RELAMPAGO-CACTI period had at least one sounding with STP < −1, but 71% of these occurred after 15 December 2018.

Previous research has found that although supercells are fairly common in proximity to the Sierras de Córdoba (e.g., Mulholland et al. 2018), tornadoes are rare in this area, with the frequency of tornadoes (and environments favorable for tornadoes) increasing to the northeast in eastern Argentina and southern Brazil (Altinger de Schwarzkopf and Rosso 1982; Brooks et al. 2003; Silva Dias 2011; Rasmussen et al. 2014).

These sounding observations from RELAMPAGO-CACTI support the findings that the environment near the SDC is not commonly favorable for tornadoes. To further examine the limiting factors for tornadoes, even though supercells are favored, we look at the individual parameters that make up the STP. As discussed above, CAPE and EVWD (which, aside from more frequent values of zero in situations where deep convection is not supported, has a distribution similar to that of the 0–6-km shear shown in Fig. 5, not shown) are routinely above the thresholds required for supercell storms that are included in the calculation of STP. Using the denominators of
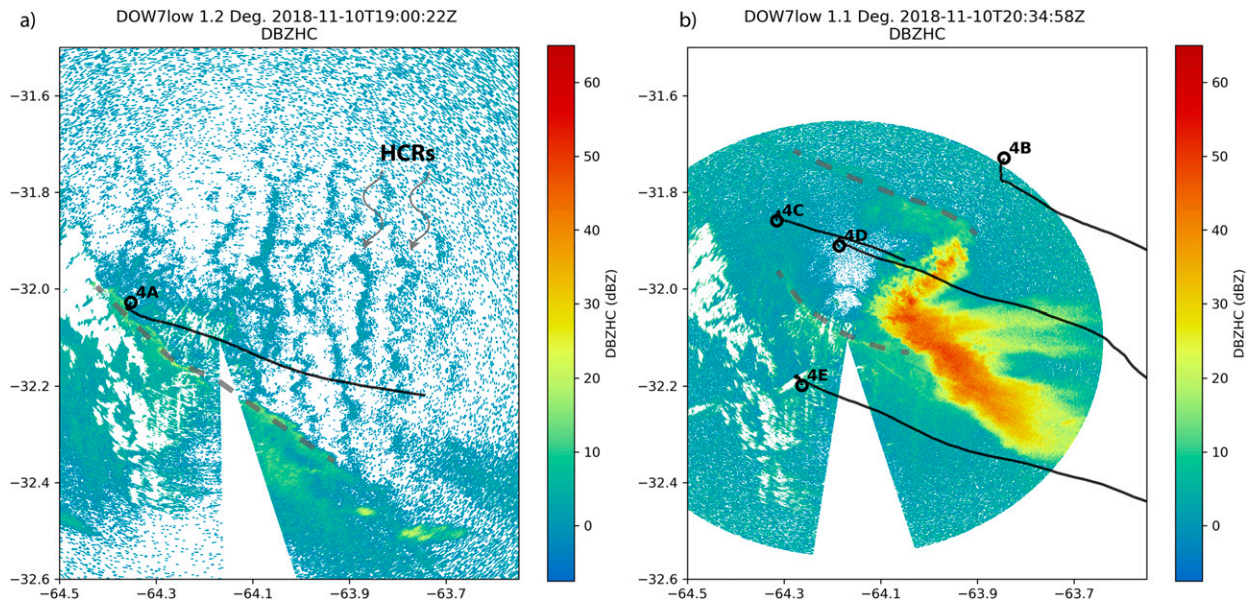

FIG. 12. DOW7 radar reflectivity factor (dBZ) at (a) 1.2° elevation at 1900 UTC and (b) 1.1° elevation at 2034 UTC 10 Nov 2018, along with launch locations and balloon/radiosonde paths of the soundings shown later in Fig. 13. Gust-front locations are shown with dashed gray lines, and horizontal convective rolls (HCRs) are identified in (a).
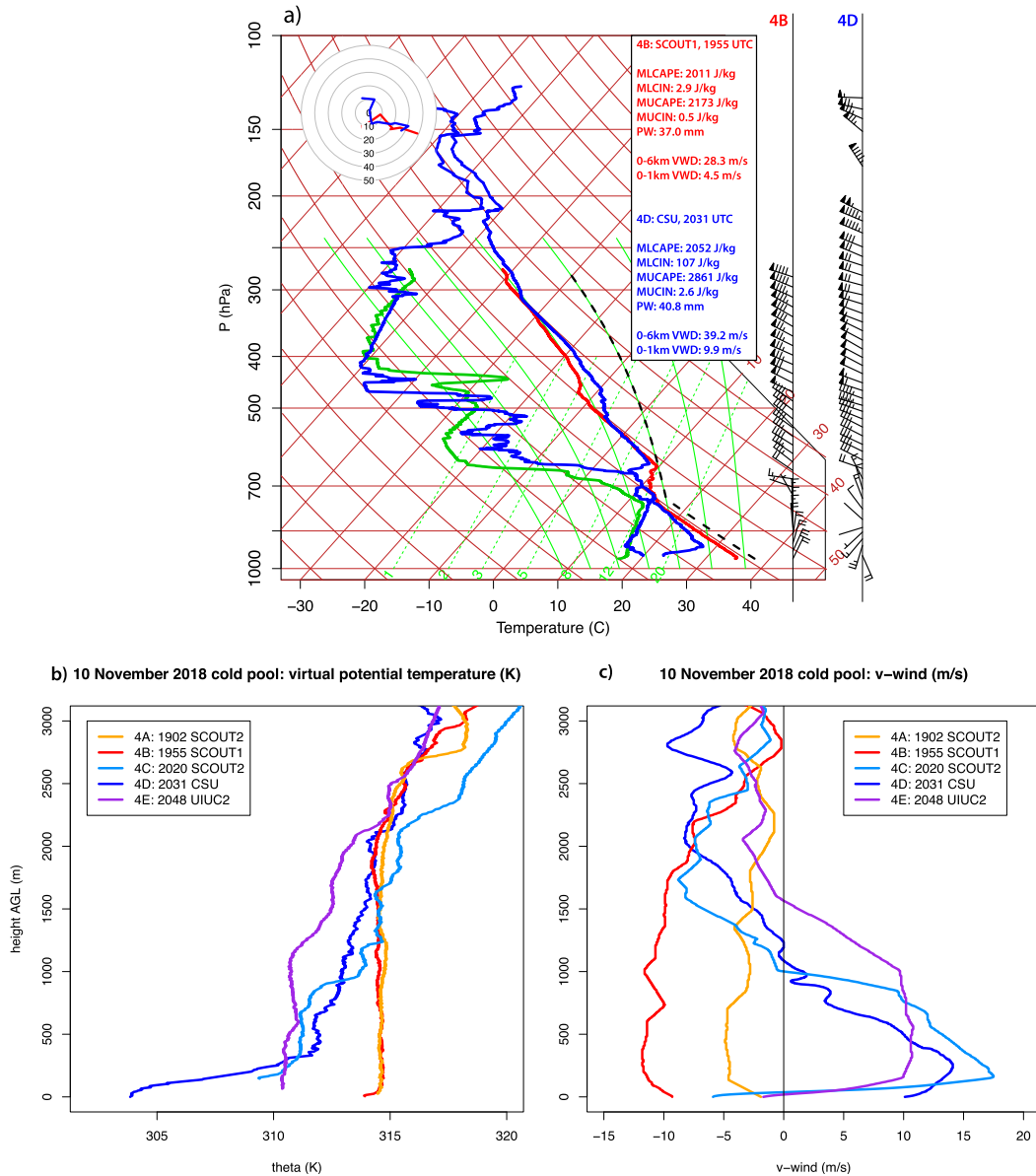
FIG. 13. (a) Skew T–log$p$ diagrams of environmental and cold-pool soundings on 10 Nov 2018. The environmental sounding (4B), with temperature in red and dewpoint in green, was taken by SCOUT2 at 1955 UTC; the cold-pool sounding (4D, temperature and dewpoint in blue) was taken by CSU at 2031 UTC. The parcel temperature (dashed black curve) is for the 1955 UTC sounding. CAPE and PW calculations for sounding 4B are for the truncated sounding and are thus underestimates. Also shown are vertical profiles of (b) virtual potential temperature and (c) meridional wind (m s^{-1}) from environmental soundings (orange and red) and cold-pool soundings (shades of blue), at the times indicated in the legend (see Fig. 12 for sounding locations).

the MLCAPE and EVWD terms in the STP as a rough guide to the magnitudes that are favorable for supercells, there were 168 soundings (of the total sample of 2712) that had both MLCAPE exceeding 1500 J kg^{-1} and EVWD exceeding 20 m s^{-1}. To assess the importance of the other three terms, which are more specifically associated with tornadoes assuming supercells are supported, we place each of them

individually as another condition in addition to MLCAPE and EVWD. Requiring MLCAPE to exceed 1500 J kg^{-1}, EVWD to exceed 20 m s^{-1}, and MLCIN to be greater than -100 J kg^{-1} (in other words, the magnitude of MLCIN is < 100 J kg^{-1}), reduces this number of soundings from 168 to 130. Requiring instead that the MLLCL height be less than 1500 m (in addition to favorable CAPE and shear) reduces the 168 soundings
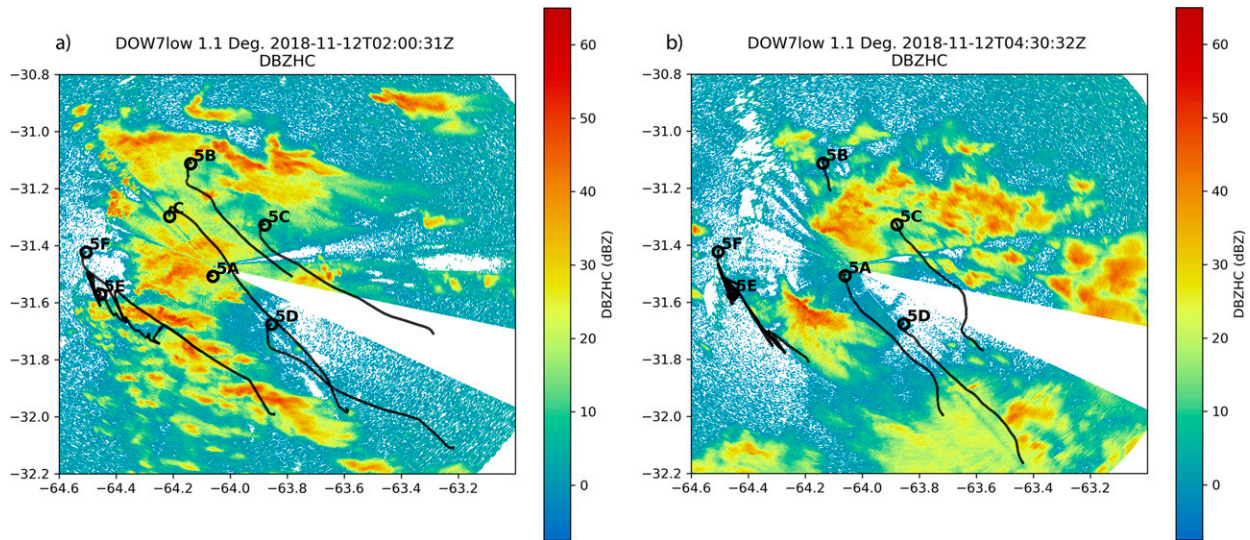
FIG. 14. DOW7 radar reflectivity factor (dBZ) at 1.1° elevation at (a) 0200 UTC and (b) 0430 UTC 12 Nov 2018, along with launch locations and balloon/radiosonde paths.

to 119. However, requiring that ESRH be less than $-100\,\mathrm{m^2\,s^{-2}}$ yields the greatest reduction, from 168 to 76 soundings. Likewise, examining 0–1-km shear, which Thompson et al. (2012) also showed to be a strong discriminator between nontornadic and tornadic supercells, shows that only 42 soundings had MLCAPE exceeding $1500\,\mathrm{J\,kg^{-1}}$, EVWD exceeding $20\,\mathrm{m\,s^{-1}}$, and 0–1-km VWD exceeding $7.5\,\mathrm{m\,s^{-1}}$. Relaxing these thresholds for each term slightly still results in the low-level shear variable being most frequently the term that is the "weak link" among the tornado parameters. These results suggest that although all of the tornado-specific variables in the STP may limit the tornado potential in different scenarios, the lack of low-level vertical wind shear (itself, and as it manifests in storm-relative helicity) is the most common factor inhibiting tornado development in the RELAMPAGO-CACTI domain. A few examples of environments that supported strong supercells but lacked the low-level shear needed for tornadogenesis will be given in section 4.

Although the RELAMPAGO-CACTI domain does not frequently support low-level rotation in supercells, severe hail-producing storms are commonly observed in this region (Mezher et al. 2012; Rasmussen et al. 2014; Kumjian et al. 2020). The significant hail parameter (SHIP), which was developed for operational use by the U.S. Storm Prediction Center (Storm Prediction Center 2020), incorporates information about MUCAPE, low-level moisture, midlevel lapse rate, and 0–6-km shear. Recent studies have confirmed the importance of both large CAPE and strong deep-layer shear for the production of large hail (e.g., Dennis and Kumjian 2017; Kumjian and Lombardo 2020). SHIP is designed to discriminate between environments with the potential to produce significant severe hail (diameter $\geq 50.8\,\mathrm{mm}$) from those only supportive of smaller hail. Values greater than approximately 1 are associated with significant severe hail (Storm Prediction Center 2020). Although no parameter

adequately distinguishes between smaller and larger hail in all situations, SHIP has been shown to have operational usefulness (e.g., Allen et al. 2020).

In the RELAMPAGO-CACTI sounding dataset, approximately 9% of all soundings had SHIP ≥ 1 (Fig. 9), and 25% of convective days had at least one sounding with SHIP ≥ 1. Seventeen of the 26 soundings with values of SHIP exceeding 2 were from IOP17 on 13–14 December; three of the others were from IOP4 on 10 November. In both of these cases, severe hail was observed within the RELAMPAGO domain; these cases will be discussed in further detail in the next section.

4. Notable cases and observations

a. Most extreme soundings for various parameters

The most extreme soundings in terms of many convective-storm parameters occurred after the primary RELAMPAGO campaign ended, on 25 and 29 January 2019. On both of these days, supercell storms were observed that contained wide overshooting tops apparent on satellite imagery (e.g., Marion et al. 2019) and maximum echo top heights observed by the CHIVO and C-Band Scanning ARM Precipitation Radar (CSAPR; Hardin et al. 2018) radars exceeding 20 km MSL.

The sounding from 2033 UTC 25 January 2019 at Córdoba (Fig. 10a) exemplifies this environment, with MUCAPE of $6376\,\mathrm{J\,kg^{-1}}$ (the ninth highest value of all soundings in the dataset), MLCAPE of $5147\,\mathrm{J\,kg^{-1}}$ (second highest), SHIP of 1.95 (34th highest), C of $123\,933\,\mathrm{m^3\,s^{-3}}$ (seventh highest), SCP of -42.6 (third largest in magnitude) and STP of -7.43 (largest in magnitude). There is ample low-level moisture, steep low- and midlevel lapse rates (including an elevated mixed layer, Ribeiro and Bosart 2017), and considerable deep-layer shear, though the low-level shear is modest. This sounding also had the most PW of any sounding in the RELAMPAGO-CACTI
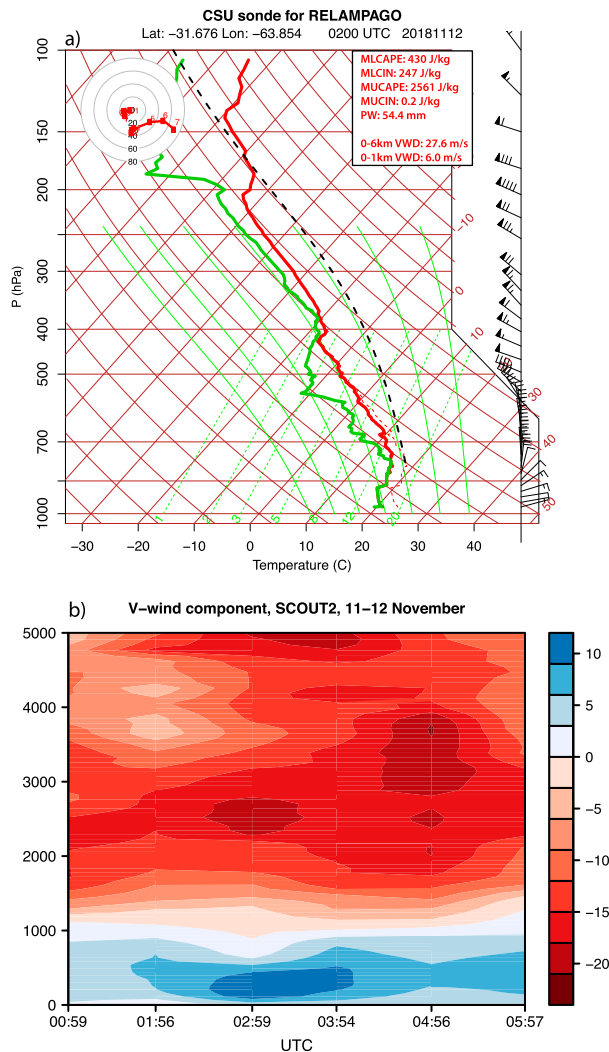
FIG. 15. (a) Skew T–logp diagram of from sounding location 5D in Fig. 14a at 0200 UTC 12 Nov 2018. (b) Time–height diagram of meridional wind (m s⁻¹) from sounding location 5A; the tick marks on the x axis indicate times of launches.

FIG. 16. DOW8 radar reflectivity factor (dBZ) at 1.0° elevation at 1800 UTC 26 Nov 2018, along with launch locations and balloon/radiosonde paths of sounding shown later in Fig. 17.

domain (64.2 mm; three soundings from Resistencia in northeastern Argentina exceeded it, and those soundings passed through convective clouds.) The 3-hourly soundings from Córdoba on this afternoon illustrate the development of the daytime boundary layer, as well as the lifting of an inversion presumably associated with large-scale ascent, yielding extreme instability and minimal inhibition by 2033 UTC (Fig. 10b). The low-level vertical wind shear also increased over the course of the day and in response to nearby convection, with the hodograph at 2033 UTC having more curvature than earlier profiles (Fig. 10c). The soundings taken from Córdoba on 29 January exhibit similar profiles (not shown), and the soundings with the most CAPE (a maximum MUCAPE of 7945 J kg⁻¹) occurred on these two days.

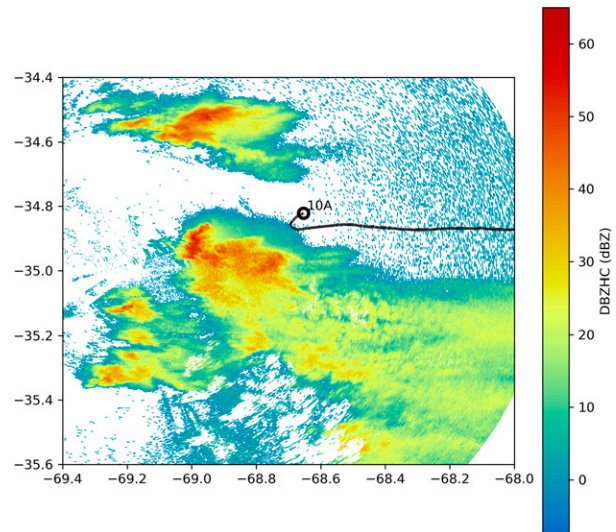On 25 January, two splitting supercells formed quickly in the unstable environment around 1630 UTC. The storm moved

northeast and became outflow dominant, growing into an MCS by 2000 UTC with many embedded intense convective cores. The storm propagated northward through the city of Córdoba, producing flash flooding. On 29 January, a line of storms initiated on the eastern slopes of the Sierras de Córdoba, around 1545 UTC, and splitting supercells moved slowly east by 1900 UTC. At 2045 UTC, these storms combined to form a large supercell-like structure that propagated northward parallel to the Sierras. Additional analysis of the storms on 25 and 29 January is included in Nesbitt et al. (2020, manuscript submitted to *Bull. Amer. Meteor. Soc.*).

During the primary RELAMPAGO campaign, the time periods with the most favorable convective environments (and in turn the most intense and organized observed convection) were 10–12 November and 13–14 December 2018. In the sections to follow, we briefly examine these and other cases that had notable sounding observations, including insights revealed from the high-frequency mobile soundings.

b. Convection initiation

One scientific focus of RELAMPAGO was the initiation of deep convection and the respective roles of the SDC and other processes in initiation. The high-frequency soundings across several successful and failed instances of convection initiation have been analyzed in detail by Nelson et al. (2020). They identified that low relative humidity at midlevels and limited convergence near the SDC, among other factors, prevented initiation in the "null" cases. Readers are directed to that manuscript for further details on convection initiation.

c. 10–12 November 2018

Multiple episodes of organized deep convection occurred in the RELAMPAGO domain, and across South America, during 10–12 November 2018. On 10 November (IOP4), a severe-
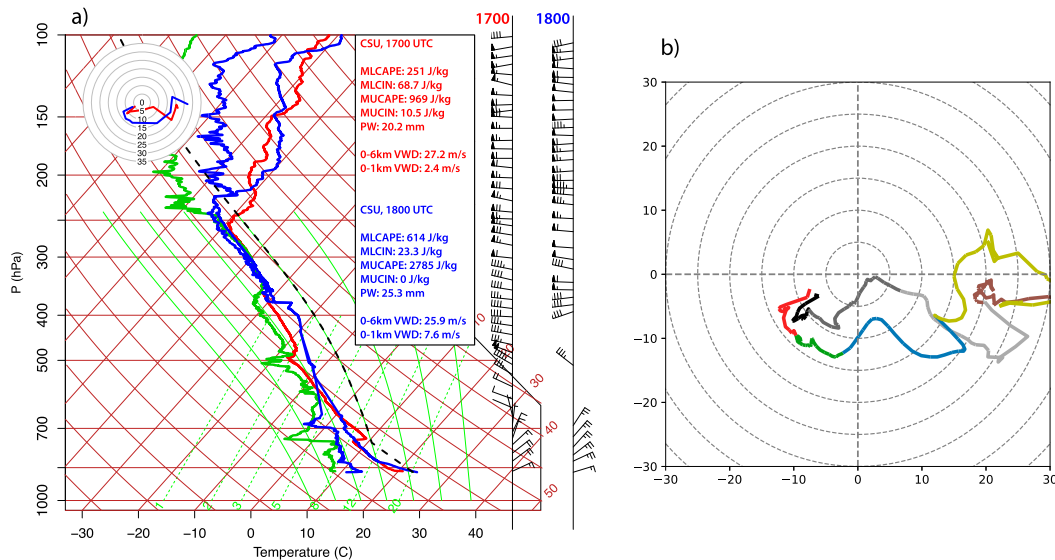
FIG. 17. (a) Skew T–log$p$ diagrams of soundings for 1700 and 1800 UTC 26 Nov 2018. The 1800 UTC radiosonde was launched from location 10A in Fig. 16; the 1700 UTC radiosonde was launched approximately 20 km south of this location. The parcel temperature (dashed black curve) is for the 1800 UTC sounding. (b) Magnified view of wind hodographs (m s^{-1}) for these two soundings, with the 1700 UTC sounding in shades of gray/brown and 1800 UTC sounding in color. Colors change at 1, 3, and 5 km AGL.

hail-producing supercell occurred that was well observed by the RELAMPAGO observing network (Trapp et al. 2020). Convection continued across Córdoba province into the early morning of 11 November, and grew upscale into an MCS that moved eastward, with another smaller MCS that followed it in the afternoon of 11 November (not shown). The RELAMPAGO observing network deployed again to sample nocturnal convection late on 11 November/early 12 November (IOP5), with convection again forming over the domain and then growing upscale into a very large mesoscale convective complex in northeastern Argentina on 12 November (Piersante et al. 2021).

The development and evolution of the convection during this time period is thoroughly analyzed by Trapp et al. (2020) and K. A. Kosiba et al. (2020, unpublished manuscript; see also https://cscenter.co.jp/icrm2019/program/data/ICRMprogram.html and https://cscenter.co.jp/icrm2019/program/data/abstracts/Session10B-01.pdf), and by Piersante et al. (2021), and the reader is referred to those articles for more comprehensive case studies, but here we focus on sounding observations of convectively generated cold pools on 10 November, and the SALLJ and associated setup for elevated convection on 11–12 November.

Soundings were launched hourly on 10 November 2018 from a network of locations east of the SDC prior to convection initiation (Fig. 11. A storm initiated at around 1930 UTC over the SDC, along an outflow boundary from convection to the south (Fig. 12a) and quickly intensified and became a supercell (Trapp et al. 2020, Fig. 12b). As the storm initiated, some sounding vehicles repositioned to attempt to collect profiles in convective updrafts or cold pools. No direct updraft soundings

were collected in this case, but three soundings from within the supercell's cold pool were obtained. Figure 13a shows a sounding at 1955 UTC (sounding 4B) in the inflow to the northeast of the developing storm, which exhibited a deep well-mixed boundary layer with sufficient CAPE and little convective inhibition. Horizontal convective rolls were observed in this environment (Fig. 12a). Vertical wind shear was sufficient for supercells (0–6-km shear was 28.3 m s^{-1}), but the low-level shear was weak (0–1-km shear of 4.5 m s^{-1}). Sounding 4C was taken immediately after the gust front passage at 2020 UTC, sounding 4D (Fig. 13a) was launched from within the cold pool at 2031 UTC, and sounding 4E at 2048 UTC from farther southwest within the cold pool. These soundings reveal that the cold pool was approximately 2 km deep based on both the cooling and the directional shift in winds (Figs. 13b,c). Sounding 4D had more pronounced near-surface cooling, with a maximum potential temperature deficit of 10 K at the surface (Fig. 13b). (The temperature data in the lowest 150 m were flagged as questionable for soundings 4C and 4E by the quality-control system). This is somewhat larger than the 4–8-K deficits observed by mobile mesonet vehicles in different parts of the cold pool; these differences may also be attributable to the challenge of defining the cold pool, considering that there was preexisting outflow that aided in convection initiation in this case (Trapp et al. 2020). Furthermore, a jet-shaped wind profile of southerly outflow winds was observed, with maximum wind speeds of 17.9 m s^{-1} between 155 and 170 m AGL in sounding 4C (Fig. 13c). Direct observations of the vertical structure of cold pools are very limited (Hitchcock et al. 2019), and this represents one of the first such sets of observations of a convectively generated cold pool in Argentina.
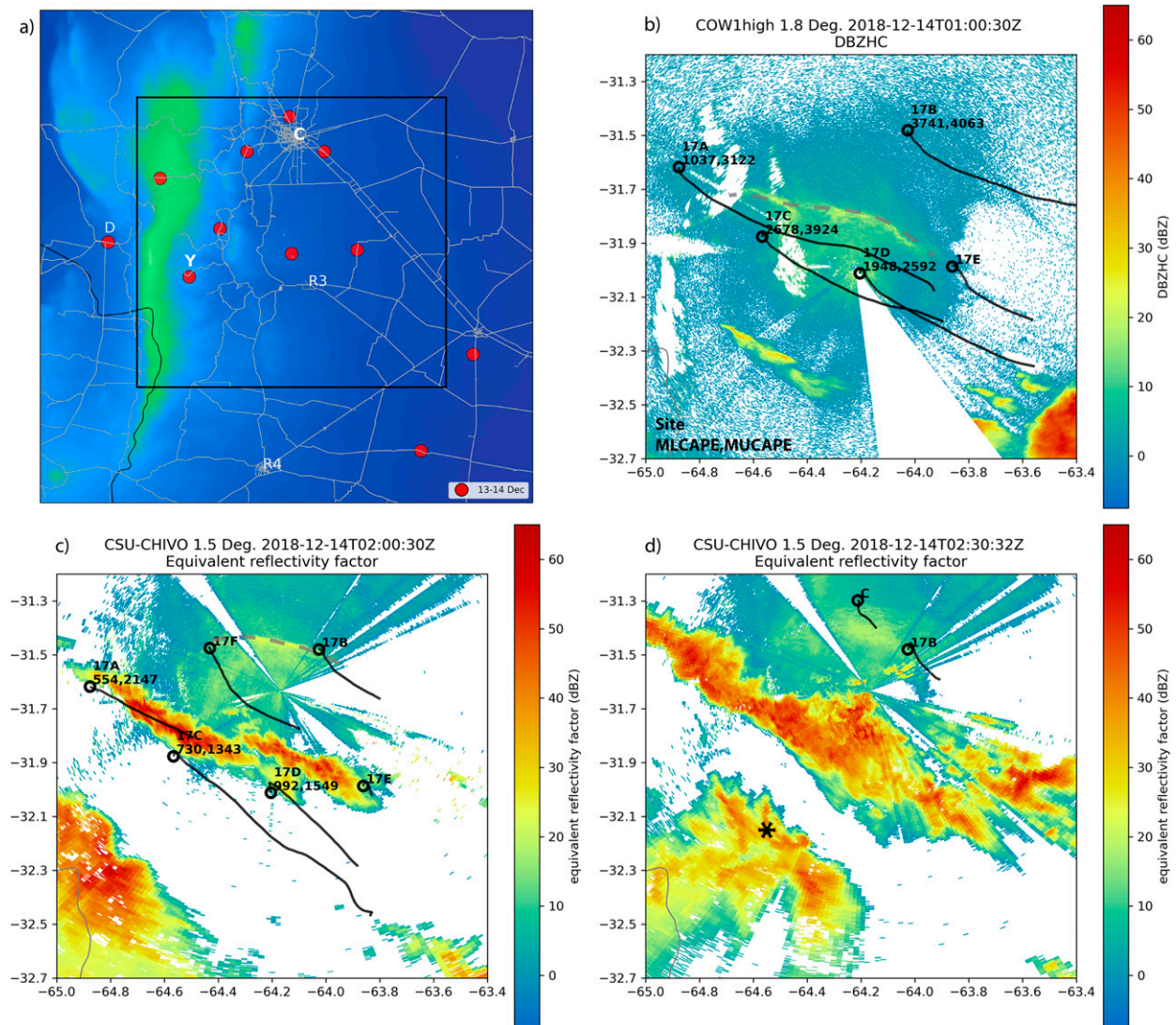
FIG. 18. (a) As in Fig. 1b, but showing launch locations during 13–14 Dec 2018. The black-outlined rectangle indicates the area shown in (b)–(d). (b) COW radar reflectivity factor (dBZ) at 1.8° elevation at 0100 UTC 14 Dec 2018; CHIVO radar reflectivity factor (dBZ) at 1.5° elevation at (c) 0200 UTC and (d) 0230 UTC 14 Dec 2018, along with launch locations and balloon/radiosonde paths. Along with the launch locations, the MLCAPE and MUCAPE (J kg^{-1}) are given, although no values are reported for soundings that did not have valid thermodynamic data above 500 hPa. Locations of an outflow boundary are indicated by the dashed gray lines in (b) and (c). The asterisk in (d) indicates Villa Amancay, where 8-cm hail was reported at approximately this time.

IOP5 sampled a nocturnal convective system on 12 November (Fig. 11. The convection had varying levels of organization throughout its lifetime, from poorly organized clusters of storms, to series of small convective lines, to storms with structures resembling supercells (Fig. 14). A network of mobile platforms launched radiosondes hourly through this event, and the environment was characterized by saturated, stable low levels, with elevated instability above (Fig. 15a). A northerly SALLJ was observed throughout the event, with the maximum wind speeds exceeding 20 m s^{-1} between 2 and 4 km AGL, above a layer of southerly or easterly winds (depending on the location) between 0 and 1 km (Fig. 15b). The SALLJ in this case was even more elevated than the average SALLJ

observed during the campaign (cf. Fig. 6) and was located much farther aloft than LLJs observed in the U.S. Great Plains as discussed in section 3c. The synoptic and mesoscale conditions leading up to the 11–12 November 2018 MCS are analyzed in Piersante et al. (2021), and these observations show that elevated nocturnal MCSs occur in Argentina with at least some similarities to those observed in the United States (e.g., Geerts et al. 2017), and warrant further investigation.

d. 26 November 2018

For two IOPs (9 and 10), a subset of the mobile observing platforms traveled west to Mendoza province on 25–26 November. On 26 November (IOP10), a supercell thunderstorm initiated
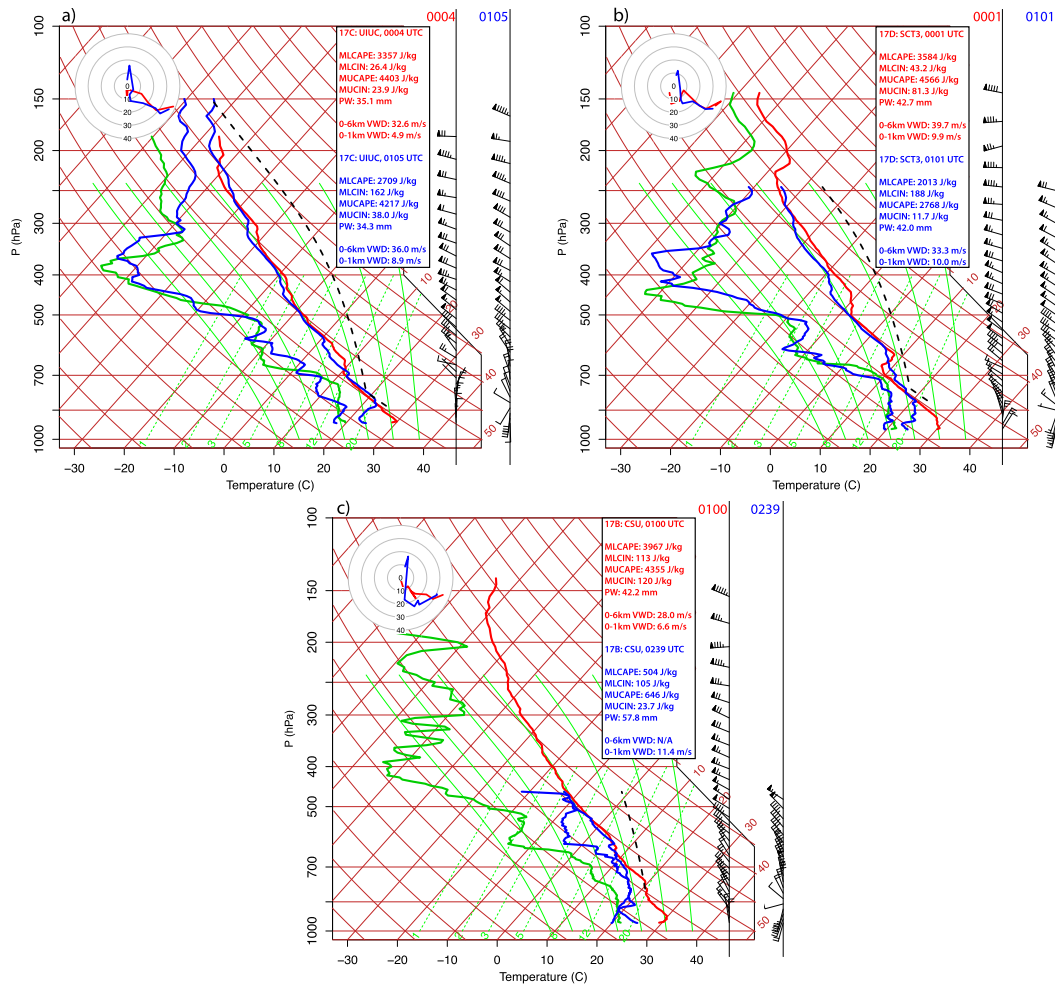
FIG. 19. (a) Skew T–logp diagrams of soundings for 0004 and 0105 UTC 14 Dec 2018 from location 17C shown in Fig. 18a. The parcel temperature (dashed black curve) is for the 0105 UTC sounding. (b) As in (a), but for sounding location 17D at 0001 and 0101 UTC. The parcel temperature is for the 0101 UTC sounding. (c) As in (a), but for sounding location 17B at 0100 and 0239 UTC. The parcel temperature is for the 0239 sounding; the thermodynamic calculations are for the truncated sounding and are thus underestimates.

and moved through the observing network. A sequence of hourly soundings revealed storm-generated effects on the vertical wind profile in the inflow to the storm. Convection initiated in the foothills of the Andes at approximately 1600 UTC, and organized into a supercell as it moved eastward (Fig. 16). Soundings from 1500, 1600 (not shown), and 1700 UTC (Fig. 17a) showed a developing unstable boundary layer, but also some inhibition for near-surface parcels. After repositioning slightly to remain ahead of the supercell, a sounding launched in the storm inflow at 1800 UTC showed that with boundary layer moistening and the removal of a capping inversion, the inhibition had been removed (Fig. 17a). In addition, what had been relatively weak low-level wind shear at 1700 UTC had become much stronger by 1800 UTC, with 0–1-km shear increasing from 2.4 to 7.6 m s^{-1}, 0–1-km SRH increasing in magnitude from −21.7 to −62.3 m^2 s^{-2}, and an enlarged hodograph (Fig. 17). These observations point to an

increase in low-level shear in the inflow region generated by the storm itself, akin to the findings of Parker (2014) and Wade et al. (2018). A wall cloud with low-level rotation was observed at around this time, although no tornado occurred (Z. Bruick 2019, personal communication). This storm produced large quantities of hail, including hailstones with diameters exceeding 4.5 cm (Soderholm et al. 2020). The SHIP in the 1800 UTC sounding was 1.77, consistent with the observation of hail nearly reaching the "significant severe" threshold of 5.08 cm. Furthermore, the subsequent sounding, taken in the wake of the storm, captured an "onion"-shaped temperature and dewpoint profile (Zipser 1977), indicative of descent within the cold pool (not shown).

e. 13–14 December 2018

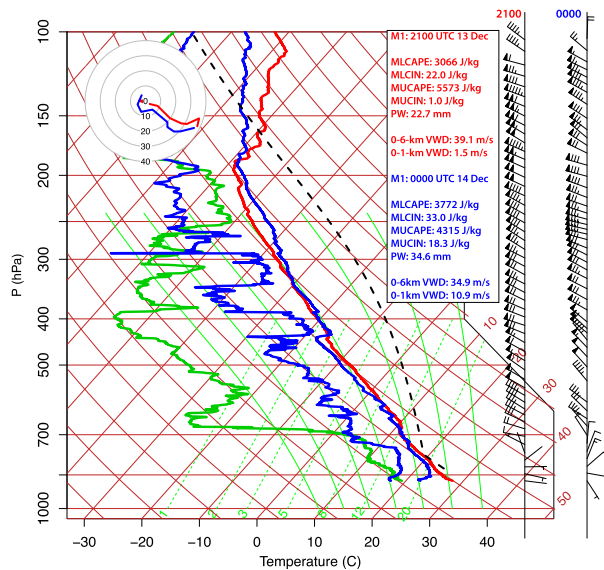For IOP17 on 13–14 December 2018, the environment was highly favorable for severe convection across Argentina, with

FIG. 20. Skew T–log$p$ diagram of soundings for 2100 UTC 13 Dec and 0000 UTC 14 Dec 2018, from the ARM site near Villa Yacanto (location shown by the "Y" in Fig. 1b). The parcel temperature (dashed black curve) is for the most unstable parcel in the 0000 UTC sounding.

the largest CAPE/shear combinations of the field campaign (Fig. 7. Soundings at 0000 UTC 14 December showed a deep well-mixed boundary layer, MLCAPE between 3000 and 4000 J kg^{-1}, and 30–40 m s^{-1} of 0–6-km shear (Figs. 18a and 19a,b). However, with no apparent lifting mechanism and a warm layer at approximately 650 hPa, there was also substantial convective inhibition, and the only convection that initiated was far to the south of the RELAMPAGO-CACTI domain. The supercells that did form to the south (one is visible in the far lower-right corner of Fig. 18a) produced a broad outflow boundary that surged northward through the RELAMPAGO domain (Fig. 18a) between 0000 and 0100 UTC 14 December. This outflow cooled the lowest ~ 1.5 km AGL, but substantial elevated instability remained, with MUCAPE exceeding 3000 J kg^{-1} behind the boundary (Figs. 19a,b). Strong southerly low-level winds within the outflow also increased the low-level vertical wind shear behind the boundary (Figs. 19a,b).

As the outflow continued to move northward through the domain, a WNW–ESE-oriented line of deep convection rapidly developed behind the gust front (Fig. 18b). This convection continued to expand and intensify (Fig. 18c), producing widespread heavy rain and flooding, and becoming a large MCS overnight (not shown). Soundings showed that the environment even to the south of this convective line remained unstable for elevated air (Fig. 18b), supporting its continued development. These profiles, which also have strong north-northwesterly winds at low- to midlevels, suggest that air was lifted over the cold pool and elevated convection was initiated. Furthermore, a sounding farther north from within the outflow that also ascended into the developing convective line at 0239 UTC shows a much deeper cold pool (approximately

2.5 km deep) yet still ample elevated instability, increased moisture, and very strong shear in the 0.5–2-km AGL layer (Fig. 19b). The final sounding of the IOP at 0304 UTC from this same location revealed a southerly wind speed of 26.8 m s^{-1} at 445 m AGL from within the convective outflow (not shown) before the radiosonde stopped transmitting data (not shown).

While this MCS was ongoing, a separate cluster of storms that developed west of the SDC moved into the domain. As this convection crossed the SDC between 0200 and 0300 UTC, it produced hail up to 8 cm in diameter (location noted in Fig. 18c). Leading up to the development of these storms and their movement into the area, soundings from the ARM site near Villa Yacanto showed a substantial increase in midlevel moisture (Fig. 20), with PW increasing by over 10 mm in the 3 h between 2100 UTC 13 December and 0000 UTC 14 December. Furthermore, the occurrence of very large hail in these storms was supported by these soundings, which had considerable CAPE, steep midlevel lapse rates, and strong deep-layer wind shear (Fig. 20). In fact, the two soundings shown in Fig. 20 had the 2nd and 3rd largest observed values of SHIP in the entire dataset, and the 0000 UTC sounding had the third largest C in the entire dataset (surpassed only by the sounding from 0001 UTC shown in Fig. 19b, and another sounding from that location an hour earlier).

5. Summary and conclusions

This study summarizes the high-frequency sounding observations that were collected during the RELAMPAGO-CACTI field campaign in Argentina from October 2018 through April 2019. An unprecedented number of radiosondes for this region were launched from both fixed and mobile stations, and the results provide some insights into why this region has some of the most intense convective storms on the planet. Moisture and instability occasionally reached very large magnitudes, and the deep-layer vertical wind shear is routinely sufficient for organized or rotating storms. The well-known South American low-level jet was frequently observed. Convective-storm parameters showed that conditions were often very favorable for supercell storms and large hail but were not frequently favorable for tornadoes, in large part because of insufficient low-level wind shear. Mobile soundings from several notable events during the field project revealed the structures of convectively generated cold pools, elevated convective systems, and convective influences on vertical wind shear.

This study only scratches the surface of what this sounding dataset can lend to convective-storm studies generally, and to comparisons between subtropical South America and other regions of intense deep convection around the world. The high resolution in space and time of the sounding dataset will enable detailed case studies and further understanding of storm processes. Furthermore, it will allow for detailed evaluation of numerical model analyses and forecasts to point to future improvements in model parameterizations and predictions.

Data availability statement. All data used in this paper were obtained from the NCAR–Earth Observing Laboratory RELAMPAGO archive (https://data.eol.ucar.edu/master_lists/generated/relampago/) and links to datasets therein.

REFERENCES

Allen, J., M. R. Kumjian, C. Nixon, R. Jewell, B. Smith, and R. Thompson, 2020: Forecast parameters for U.S. hail occurrence and size. *30th Conf. on Weather Analysis and Forecasting/26th Conf. on Numerical Weather Prediction*, Boston, MA, Amer. Meteor. Soc., 1A.4, https://ams.confex.com/ams/2020Annual/webprogram/Paper368490.html.

Altinger de Schwarzkopf, M., and L. Rosso, 1982: Severe storms and tornadoes in Argentina. *12th Conf. on Severe Local Storms*, San Antonio, TX, Amer. Meteor. Soc., 192–196.

Arias, I., and V. Chandrasekar, 2019: CSU C-Band Radar Data, version 1.0. Accessed 15 June 2020, https://doi.org/10.26023/DA1G-MCNC-YB0F.

Blumberg, W. G., K. T. Halbert, T. A. Supinie, P. T. Marsh, R. L. Thompson, and J. A. Hart, 2017: SHARPpy: An open-source sounding analysis toolkit for the atmospheric sciences. *Bull. Amer. Meteor. Soc.*, **98**, 1625–1636, https://doi.org/10.1175/BAMS-D-15-00309.1.

Bonner, W. D., 1968: Climatology of the low level jet. *Mon. Wea. Rev.*, **96**, 833–850, https://doi.org/10.1175/1520-0493(1968)096<0833:COTLLJ>2.0.CO;2.

Brooks, H. E., J. W. Lee, and J. P. Craven, 2003: The spatial distribution of severe thunderstorm and tornado environments from global reanalysis data. *Atmos. Res.*, **67–68**, 73–94, https://doi.org/10.1016/S0169-8095(03)00045-0.

Bruick, Z. S., K. L. Rasmussen, and D. J. Cecil, 2019: Subtropical South American hailstorm characteristics and environments. *Mon. Wea. Rev.*, **147**, 4289–4304, https://doi.org/10.1175/MWR-D-19-0011.1.

Carroll, B. J., B. B. Demoz, and R. Delgado, 2019: An overview of low-level jet winds and corresponding mixed layer depths during PECAN. *J. Geophys. Res. Atmos.*, **124**, 9141–9160, https://doi.org/10.1029/2019JD030658.

Cecil, D. J., and C. B. Blankenship, 2012: Toward a global climatology of severe hailstorms as estimated by satellite passive microwave imagers. *J. Climate*, **25**, 687–703, https://doi.org/10.1175/JCLI-D-11-00130.1.

Center for Severe Weather Research, 2019: CSWR RELAMPAGO dataset, version 1.0. Accessed 15 June 2020, https://data.eol.ucar.edu/dataset/553.055.

Craven, J. P., R. E. Jewell, and H. E. Brooks, 2002: Comparison between observed convective cloud-base heights and lifting condensation level for two different lifted parcels. *Wea. Forecasting*, **17**, 885–890, https://doi.org/10.1175/1520-0434(2002)017<0885:CBOCCB>2.0.CO;2.

——, H. E. Brooks, and J. A. Hart, 2004: Baseline climatology of sounding derived parameters associated with deep, moist convection. *Natl. Wea. Dig.*, **28**, 13–24.

de Elía, R., L. Vidal, P. Lohigorry, R. Mezher, and M. Rugna, 2017: El SMN y la red argentina de radares meteorológicos. SMN Nota Técnica SMN 2017-39, 21 pp., http://repositorio.smn.gob.ar/bitstream/handle/20.500.12160/625/Nota_Tecnica_SMN_2017-39.pdf?sequence=1&isAllowed=y.

Dennis, E. J., and M. R. Kumjian, 2017: The impact of vertical wind shear on hail growth in simulated supercells. *J. Atmos. Sci.*, **74**, 641–663, https://doi.org/10.1175/JAS-D-16-0066.1.

Doswell, C. A., III, and D. M. Schultz, 2006: On the use of indices and parameters in forecasting severe storms. *Electron. J. Severe Storms Meteor.*, **1**(3), https://www.ejssm.org/ojs/index.php/ejssm/article/viewArticle/11/12.

Geerts, B., and Coauthors, 2017: The 2015 Plains elevated convection at night field project. *Bull. Amer. Meteor. Soc.*, **98**, 767–786, https://doi.org/10.1175/BAMS-D-15-00257.1.

Gensini, V. A., and W. S. Ashley, 2011: Climatology of potentially severe convective environments from the North American Regional Reanalysis. *Electron. J. Severe Storms Meteor.*, **6** (8), https://www.ejssm.org/ojs/index.php/ejssm/article/viewArticle/85.

Hardin, J., A. Hunzinger, E. Schuman, A. Matthews, N. Bharadwaj, A. Varble, K. Johnson, and S. Giangrande, 2018: C-Band Scanning ARM Precipitation Radar (CSAPR2CFRPPIQC). Atmospheric Radiation Measurement (ARM) user facility, accessed 13 June 2020, https://doi.org/10.5439/1615604.

Helmus, J., and S. Collis, 2016: The Python ARM Radar Toolkit (Py-ART), a library for working with weather radar data in the Python programming language. *J. Open Res. Software*, **4**, e25, https://doi.org/10.5334/jors.119.

Hitchcock, S. M., R. S. Schumacher, G. R. Herman, M. C. Coniglio, M. D. Parker, and C. L. Ziegler, 2019: Evolution of pre- and postconvective environmental profiles from mesoscale convective systems during PECAN. *Mon. Wea. Rev.*, **147**, 2329–2354, https://doi.org/10.1175/MWR-D-18-0231.1.

Holdridge, D., J. Kyrouac, and E. Keeler, 2018: Balloon-borne sounding system (SONDEWNPN). Atmospheric Radiation Measurement (ARM) user facility, accessed 27 May 2020, https://doi.org/10.5439/1021460.

Houze, R. A., Jr., K. L. Rasmussen, M. D. Zuluaga, and S. R. Brodzik, 2015: The variable nature of convection in the tropics and subtropics: A legacy of 16 years of the tropical rainfall measuring mission satellite. *Rev. Geophys.*, **53**, 994–1021, https://doi.org/10.1002/2015RG000488.

Johns, R. H., and C. A. Doswell III, 1992: Severe local storms forecasting. *Wea. Forecasting*, **7**, 588–612, https://doi.org/10.1175/1520-0434(1992)007<0588:SLSF>2.0.CO;2.

Kumjian, M. R., and K. Lombardo, 2020: A hail growth trajectory model for exploring the environmental controls on hail size: Model physics and idealized tests. *J. Atmos. Sci.*, **77**, 2765–2791, https://doi.org/10.1175/JAS-D-20-0016.1.

——, and Coauthors, 2020: Gargantuan hail in Argentina. *Bull. Amer. Meteor. Soc.*, **101**, E1241–E1258, https://doi.org/10.1175/BAMS-D-19-0012.1.

Liu, C., and E. J. Zipser, 2015: The global distribution of largest, deepest, and most intense precipitation systems. *Geophys. Res. Lett.*, **42**, 3591–3595, https://doi.org/10.1002/2015GL063776.

Marion, G. R., R. J. Trapp, and S. W. Nesbitt, 2019: Using overshooting top area to discriminate potential for large, intense tornadoes. *Geophys. Res. Lett.*, **46**, 12 520–12 526, https://doi.org/10.1029/2019GL084099.

Markowski, P., and Y. Richardson, 2010: *Mesoscale Meteorology in Midlatitudes.* Wiley-Blackwell, 430 pp.

Matsudo, C., and P. Salio, 2011: Severe weather reports and proximity to deep convection over Northern Argentina. *Atmos. Res.*, **100**, 523–537, https://doi.org/10.1016/j.atmosres.2010.11.004.

Mezher, R. N., M. Doyle, and V. Barros, 2012: Climatology of hail in Argentina. *Atmos. Res.*, **114–115**, 70–82, https://doi.org/10.1016/j.atmosres.2012.05.020.

Montini, T. L., C. Jones, and L. M. V. Carvalho, 2019: The South American low-level jet: A new climatology, variability, and changes. *J. Geophys. Res. Atmos.*, **124**, 1200–1218, https://doi.org/10.1029/2018JD029634.

Mulholland, J. P., S. W. Nesbitt, R. J. Trapp, K. L. Rasmussen, and P. V. Salio, 2018: Convective storm life cycle and environments near the Sierras de Córdoba, Argentina. *Mon. Wea. Rev.*, **146**, 2541–2557, https://doi.org/10.1175/MWR-D-18-0081.1.

Nelson, T. C., J. Marquis, A. Varble, and K. Friedrich, 2020: Radiosonde observations of environments supporting deep moist convection initiation during RELAMPAGO-CACTI. *Mon. Wea. Rev.*, **149**, 289–309, https://doi.org/10.1175/MWR-D-20-0148.1.

Nesbitt, S. W., R. Cifelli, and S. A. Rutledge, 2006: Storm morphology and rainfall characteristics of TRMM precipitation features. *Mon. Wea. Rev.*, **134**, 2702–2721, https://doi.org/10.1175/MWR3200.1.

——, and Coauthors, 2021: A storm safari in Argentina: Proyecto RELAMPAGO, *Bull. Amer. Meteor. Soc.*, https://doi.org/10.1175/BAMS-D-20-0029.1, in press.

Nowotarski, C. J., J. M. Peters, and J. P. Mulholland, 2020: Evaluating the effective inflow layer of simulated supercell updrafts. *Mon. Wea. Rev.*, **148**, 3507–3532, https://doi.org/10.1175/MWR-D-20-0013.1.

Oliveira, M. I., E. L. Nascimento, and C. Kannenberg, 2018: A new look at the identification of low-level jets in South America. *Mon. Wea. Rev.*, **146**, 2315–2334, https://doi.org/10.1175/MWR-D-17-0237.1.

Parker, M. D., 2014: Composite VORTEX2 supercell environments from near-storm soundings. *Mon. Wea. Rev.*, **142**, 508–529, https://doi.org/10.1175/MWR-D-13-00167.1.

Piersante, J. O, K. L. Rasmussen, R. S. Schumacher, A. K. Rowe, and L. A. McMurdie, 2021: A synoptic evolution comparison of the smallest and largest MCSs in subtropical South America between spring and summer. *Mon. Wea. Rev.*, https://doi.org/10.1175/MWR-D-30-0208.1, in press.

Rasmussen, K. L., M. D. Zuluaga, and R. A. Houze Jr., 2014: Severe convection and lightning in subtropical South America. *Geophys. Res. Lett.*, **41**, 7359–7366, https://doi.org/10.1002/2014GL061767.

——, M. M. Chaplin, M. D. Zuluaga, and R. A. Houze, 2015: Contribution of extreme convective storms to rainfall in South America. *J. Hydrometeor.*, **17**, 353–367, https://doi.org/10.1175/JHM-D-15-0067.1.

Ribeiro, B., and L. F. Bosart, 2017: Elevated mixed layers and associated severe thunderstorm environments in South and North America. *Mon. Wea. Rev.*, **146**, 3–28, https://doi.org/10.1175/MWR-D-17-0121.1.

——, and L. Machado, 2019: Brazil Sao Borja Radiosonde Data, version 1.0. UCAR/NCAR–Earth Observing Laboratory, accessed 27 May 2020, https://doi.org/10.26023/416N-161D-BC09.

Romatschke, U., and R. A. Houze, 2010: Extreme summer convection in South America. *J. Climate*, **23**, 3761–3791, https://doi.org/10.1175/2010JCLI3465.1.

Salio, P., M. Nicolini, and E. J. Zipser, 2007: Mesoscale convective systems over southeastern South America and their relationship with the South American low-level jet. *Mon. Wea. Rev.*, **135**, 1290–1309, https://doi.org/10.1175/MWR3305.1.

Sasaki, C., A. K. Rowe, L. McMurdie, and K. L. Rasmussen, 2021: Analysis of the South American low-level jet during the RELAMPAGO campaign. *Mesoscale Processes Across Scales Symp.*, 331, Amer. Meteor. Soc., https://ams.confex.com/ams/101ANNUAL/meetingapp.cgi/Paper/379293.

Schumacher, R., 2019: CSU mobile radiosonde data, version 1.0. UCAR/NCAR–Earth Observing Laboratory, accessed 27 May 2020, https://doi.org/10.26023/3QGG-JQKS-AF0G.

Servicio Meteorologico Nacional—Argentina, 2019: SMN radiosonde data, version 1.0. UCAR/NCAR–Earth Observing Laboratory, accessed 27 May 2020, https://doi.org/10.26023/E8MP-0GD3-4903.

Silva Dias, M. A. F., 2011: An increase in the number of tornado reports in Brazil. *Wea. Climate Soc.*, **3**, 209–217, https://doi.org/10.1175/2011WCAS1095.1.

Smith, E. N., J. G. Gebauer, P. M. Klein, E. Fedorovich, and J. A. Gibbs, 2019: The Great Plains low-level jet during PECAN: Observed and simulated characteristics. *Mon. Wea. Rev.*, **147**, 1845–1869, https://doi.org/10.1175/MWR-D-18-0293.1.

Soderholm, J. S., M. R. Kumjian, N. McCarthy, P. Maldonado, and M. Wang, 2020: Quantifying hail size distributions from the sky—Application of drone aerial photogrammetry. *Atmos. Meas. Tech.*, **13**, 747–754, https://doi.org/10.5194/amt-13-747-2020.

Song, J., K. Liao, R. L. Coulter, and B. M. Lesht, 2005: Climatology of the low-level jet at the Southern Great Plains atmospheric boundary layer experiments site. *J. Appl. Meteor.*, **44**, 1593–1606, https://doi.org/10.1175/JAM2294.1.

Storm Prediction Center, 2020: Significant hail parameter. Accessed 28 July 2020, https://www.spc.noaa.gov/exper/mesoanalysis/help/help_sigh.html.

Thompson, R. L., R. Edwards, J. A. Hart, K. L. Elmore, and P. Markowski, 2003: Close proximity soundings within supercell environments obtained from the Rapid Update Cycle. *Wea. Forecasting*, **18**, 1243–1261, https://doi.org/10.1175/1520-0434(2003)018<1243:CPSWSE>2.0.CO;2.

——, ——, and C. M. Mead, 2004: An update to the supercell composite and significant tornado parameters. *22nd Conf. on Severe Local Storms*, Hyannis, MA, Amer. Meteor. Soc., P8.1, https://ams.confex.com/ams/11aram22sls/techprogram/paper_82100.htm.

——, C. M. Mead, and R. Edwards, 2007: Effective storm-relative helicity and bulk shear in supercell thunderstorm environments. *Wea. Forecasting*, **22**, 102–115, https://doi.org/10.1175/WAF969.1.

——, B. T. Smith, J. S. Grams, A. R. Dean, and C. Broyles, 2012: Convective modes for significant severe thunderstorms in the contiguous United States. Part II: Supercell and QLCS tornado environments. *Wea. Forecasting*, **27**, 1136–1154, https://doi.org/10.1175/WAF-D-11-00116.1.

Trapp, R. J., D. J. Stensrud, M. C. Coniglio, R. S. Schumacher, M. E. Baldwin, S. Waugh, and D. T. Conlee, 2016: Mobile radiosonde deployments during the Mesoscale Predictability Experiment (MPEX): Rapid and adaptive sampling of upscale convective feedbacks. *Bull. Amer. Meteor. Soc.*, **97**, 329–336, https://doi.org/10.1175/BAMS-D-14-00258.1.

——, and Coauthors, 2020: Multiple-platform and multiple-Doppler radar observations of a supercell thunderstorm in South America during RELAMPAGO. *Mon. Wea. Rev.*, **148**, 3225–3241, https://doi.org/10.1175/MWR-D-20-0125.1.

UCAR/NCAR–Earth Observing Laboratory, 2020a: Multi-network composite 5 mb vertical resolution sounding composite, version 1.3. Accessed 27 May 2020, https://doi.org/10.26023/EXZJ-XBEV-KV05.

——, 2020b: Multi-network composite highest resolution radiosonde data, version 1.3. Accessed 27 May 2020, https://doi.org/10.26023/GKFF-YNBJ-BV14.

Varble, A. C., and Coauthors, 2021: Utilizing a storm-generating hotspot to study convective cloud transitions: The CACTI experiment. *Bull. Amer. Meteor. Soc.*, https://doi.org/10.1175/BAMS-D-20-0030.1, in press.

Vera, C., and Coauthors, 2006: The South American low-level jet experiment. *Bull. Amer. Meteor. Soc.*, **87**, 63–78, https://doi.org/10.1175/BAMS-87-1-63.

Wade, A. R., M. C. Coniglio, and C. L. Ziegler, 2018: Comparison of near- and far-field supercell inflow environments using radiosonde observations. *Mon. Wea. Rev.*, **146**, 2403–2415, https://doi.org/10.1175/MWR-D-17-0276.1.

Whiteman, C. D., X. Bian, and S. Zhong, 1997: Low-level jet climatology from enhanced rawinsonde observations at a site in the Southern Great Plains. *J. Appl. Meteor.*, **36**, 1363–1376, https://doi.org/10.1175/1520-0450(1997)036<1363:LLJCFE>2.0.CO;2.

Wurman, J., and K. Kosiba, 2021: FARM-data-RELAMPAGO (version 1) [Data set]. Center for Severe Weather Research, accessed 15 June 2020, https://doi.org/10.48514/NK1P-7J11.

Zipser, E. J., 1977: Mesoscale and convective-scale downdrafts as distinct components of squall-line structure. *Mon. Wea. Rev.*, **105**, 1568–1589, https://doi.org/10.1175/1520-0493(1977)105<1568:MACDAD>2.0.CO;2.

——, D. J. Cecil, C. Liu, S. W. Nesbitt, and D. P. Yorty, 2006: Where are the most intense thunderstorms on Earth? *Bull. Amer. Meteor. Soc.*, **87**, 1057–1072, https://doi.org/10.1175/BAMS-87-8-1057.